Department of Mechanical Engineering
University of New Brunswick
Fredericton, N.B.

CA1
DTC 801
8-
T112
c.2

TP 7514E

TANK CAR THERMAL RESPONSE ANALYSIS: FINAL REPORT, VOLUME 2 TRANSIENT NATURAL CONVECTION IN A PARTIALLY FILLED HORIZONTAL CYLINDER

N.U. Aydemir, J.E.S.Venart, A.C.M.Sousa

Prepared For:

TRANSPORT CANADA
TRANSPORTATION DEVELOPMENT CENTER
Montreal, Quebec H3A 2R3

Prepared By:

University of New Brunswick
Department of Mechanical Engineering
P.O. Box 4400
Fredericton, NB E3B 5A3

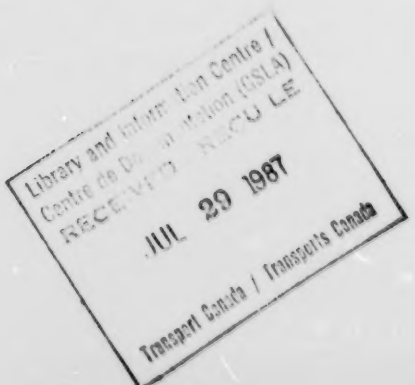
Library and Information Centre /
Centre de Documentation (GSLA)
RECEIVED / REÇU LE
JUL 29 1987
Transport Canada / Transports Canada

THE CONTENTS OF THIS REPORT REFLECT
THE VIEWS OF THE CONTRACTOR AND NOT
NECESSARILY THE OFFICIAL VIEWS OR
POLICIES OF THE TRANSPORTATION
DEVELOPMENT CENTER

REPORT DOCUMENTATION FORM

1. Transport Canada Report No.	2. TDC Project No.	3. Recipient's Catalogue No.
TP 7514E	4727	

4. Title and Subtitle	5. Report Date
Tank Car Thermal Response Analysis: Volume 2 Transient Natural Convection in a Partially Filled Horizontal Cylinder	6. Performing Organization Report No. UNB-ME-TF 25

7. Author(s)	8. Transport Canada File No.
N.U. Aydemir, J.E.S. Venart, A.C.M. Sousa	D1465-302-2

9. Performing Organization Name and Address	10. DSS File No.
Fire Science Centre University of New Brunswick P.O. Box 4400 Fredericton, N.B. E3B 5A3	11SD.T8200-2-2509
	11. DSS or Transport Canada Contract No. OSD82-00085

12. Sponsoring Agency Name and Address	13. Type of Report and Period Covered
Transportation Development Centre (TDC) Guy Favreau Complex 200 Dorchester Blvd. West, Suite 601, West Tower Montreal, Quebec H2Z 1X4	14. Sponsoring Agency Code TDC 4727

15. Supplementary Notes	16. TDC Project Officer
See also "Tank Car Thermal Response Analysis: Executive Summary", by J.E.S. Venart, March 1985, TP 6809E.	**D.W. Dibble**

17. Abstract

The problem of transient natural convection in a partially filled, uniformly heated horizontal cylinder is studied. Two methods are used to solve the governing equations of motion. In one of them, the model equations are rewritten in their integral forms and closed expressions are obtained for the thermal stratification phenomena inside the cylinder using a new stability criteria proposed for the free convective boundary layer along the walls. The predictions compare favorably with the experimental data available. Secondly, the differential equations of motion are integrated numerically with finite differences using a technique of coordinate transformation. The computations compare satisfactorily with the experimental data for completely filled cylindrical tanks. Qualitative agreement is obtained for a partially filled cylinder with respect to the flow pattern.

18. Key Words	19. Distribution Statement
Rail, Tank Car, Thermal, Heat, Energy, Convection, Transfer	Limited number of copies available from the Transportation Development Centre

20. Security Classification (of this report)	21. Security Classification (of this page)	22. No of Pages	23. Price
Unclassified	Unclassified	101	---

FORMULE DE DOCUMENTATION POUR RAPPORT

1. N° du rapport Transports Canada	2. N° de l'étude — CDT	3. N° de catalogue du destinataire
TP 7514E	4727	

4. Titre et sous-titre	5. Date du rapport
Tank Car Thermal Response Analysis: Volume 2 Transient Natural Convection in a Partially Filled Horizontal Cylinder	6. N° du rapport de l'organisme exécutant: UNB-ME-TF 25

7. Auteur(s)	8. N° de dossier Transports Canada
N.U. Aydemir, J.E.S. Venart, A.C.M. Sousa	D1465-302-2

9. Nom et adresse de l'organisme exécutant	10. N° de dossier — ASC
Fire Science Centre Université du Nouveau-Brunswick C.P. 4400 Fredericton, N.B. E3B 5A3	11SD.T8200-2-2509 11. N° de contrat — ASC ou Transports Canada: OSD82-00085

12. Nom et adresse de l'organisme parrain	13. Genre de rapport et période visée
Centre de développement des transports (CDT) Complexe Guy-Favreau 200 ouest, boul. Dorchester, Suite 601, Tour Ouest Montréal, Québec H2Z 1X4	14. Code de l'organisme parrain: CDT 4727

15. Remarques additionnelles	16. Agent de projet — CDT
Voir aussi "Tank Car Thermal Response Analysis: Executive Summary", par J.E.S. Venart, mars 1985, TP 6809E.	**D.W. Dibble**

17. Résumé

Nous avons étudié la convection naturelle transitoire dans un cylindre horizontal partiellement rempli et chauffé uniformément. Deux méthodes ont été utilisées pour résoudre les équations du mouvement. Avec la première, les équations du modèle sont transformées en équations intégrales et l'on obtient des expressions fermées pour le phénomène de stratification thermique à l'intérieur du cylindre en utilisant un nouveau critère de stabilité proposé pour la couche limite de convection libre le long des parois. Les valeurs calculées sont en bonne concordance avec les valeurs mesurées disponibles. Avec la seconde méthode, les équations différentielles du mouvement sont intégrées numériquement avec des incréments finis en utilisant une transformation de coordonnées. Les valeurs calculées sont en concordance satisfaisante avec les valeurs mesurées pour les réservoirs cylindriques pleins à capacité. Avec les cylindres remplis partiellement, on obtient une concordance acceptable pour les caractéristiques d'écoulement.

18. Mots-clés	19. Diffusion
Rail, wagon-citerne, thermique, chaleur, énergie, convection, transfert	Le Centre de développement des transports dispose d'un nombre limité d'exemplaires.

20. Classification de sécurité (de ce rapport)	21. Classification de sécurité (de cette page)	22. Nombre de pages	23. Prix
non classifié	non classifiée	101	---

TABLE OF CONTENTS

		PAGE
I	INTRODUCTION	1
	1.1 Objectives	1
	1.2 The Physical Phenomena	5
	1.3 The Mathematical Model	10
	1.4 Possible Solutions of the Governing Equations of Motion	13
II	INTEGRAL ANALYSIS	15
	2.1 Introduction	15
	2.2 Analysis	16
	2.3 An Exact Solution of the Integral Equations of Motion	20
III	A THERMAL STRATIFICATION MODEL	28
	3.1 Introduction	28
	3.2 A Model for Thermal Stratification	31
	3.3 Approximate Analysis of Hydrodynamic Stability of a Boundary Layer on a Concave Surface	33
	3.4 Final Describing Equations	36
	3.5 Modifications of Flow Properties for a Porous Boundary Layer	38
	3.6 Effects of External Stratification on the Boundary Layer	39
	3.7 Results and Discussion	41
IV	FINITE DIFFERENCE SOLUTIONS	46
	4.1 Introduction	46
	4.2 The Difficulties Associated With the Geometry and A Possible Approach	47
	4.3 The Boundary Conditions	53
	4.4 Discretization in the ζ-η Plane; Disadvantages and Advantages	58
	4.5 Solution Method and Algorithm	59
	4.6 Test Runs	61
	4.7 Heat Lines	78
	4.8 Conclusions	84
REFERENCES		88
APPENDIX A	PERTURBATION SOLUTIONS FOR EXTERNAL STRATIFICATIONS	91
APPENDIX B	TRANSFORMED EQUATIONS OF MOTION	95
APPENDIX C	DISCRETIZED EQUATIONS	97
APPENDIX D	COMPUTATIONAL FLOW CHART	99

LIST OF FIGURES

Figure		Page
1	Partially filled horizontal cylinder heated from the side	2
2	Physical picture	7
3	Transient development of vertical temperature profiles for Q = 20 Kw/sq.m, 92% fill, without EXPLOSAFE	9
4.a	Comparison of velocity scales	23
4.b	Boundary layer growth	23
4.c	Variation of mean Nusselt number with Prandtl number	25
5.a,b	Local variation of Nusselt number with position along the wall, (a) Pr = 1.0, (b) Pr = 0.7	26
6	Normal forces on a fluid element. Tangential forces are not shown	34
7	Momentum boundary layer for various degrees of external stratification (curves 1,2,3 and 4 are defined in text, eqn. 3.19)	42
8	80% fill, with 1" EXPLOSAFE. Transient development of vertical temperature gradient (Q = 40 Kw/sq.m)	43
9	85% fill, without EXPLOSAFE. Transient development of vertical temperature gradient (Q = 20 Kw/sq.m)	43
10.a	Physical plane	50
10.b	Mathematical plane	50
11	Grid system for wall vorticity (at left i = 1)	55
12	Velocity profiles for Pr = 19950, Gr = 1.1 . .	62

LIST OF FIGURES - Continued

Figure		Page
13	Temperature profiles for Pr = 19950, Gr = 1.1	63
14.a	Velocity vector plot after steady state computations for Pr = 19950, Gr = 1.1, 40 x 40 mesh	64
14.b	Enlarged central core with two rotating eddies	64
15	Temperature profiles for Pr = 0.7, $Gr = 4.5 \times 10^4$	65
16	Velocity profiles for Pr = 0.7, $Gr = 4.5 \times 10^4$	66
17.a	Steady state isothermals for Pr = 19950, Gr = 1.1	68
17.b	Steady state isothermals for Pr = 0.7, $Gr = 4.5 \times 10^4$	69
18.a, b, c	Streamlines in transient computation, . . .	70
	Pr = 6380, $Gr^*_R = 114$, (a) t = 0.7 mins, . .	71
	(b) t = 3.3 mins, (c) t = 4.6 mins	72
19.a, b, c	Isotherms in transient computation, ...	74
	Pr = 6380, $Gr^*_R = 114$, (a) t = 0.7 mins, . .	75
	(b) t = 3.3 mins, (c) t = 4.6 mins	76
20	Transient central velocities for Pr = 6380, $Gr^*_R = 114$, ($\phi = 180^\circ$)	77
21	Experimental flow pattern for 60% full tank, Pr = 6380, $Gr^*_R \cong 35$	79
22.a, b	Heat lines for Pr = 6380, $Gr^*_R = 114$, (a) t = 0.7 mins, (b) t = 4.6 mins	83
A.1	The geometry of Explosafe mesh (style 2) . .	92
B.1	First three solutions for the dimensionless velocity profiles, no external stratification	96
B.2	First three solutions for the dimensionless velocity profiles for $A = \phi + \phi^2/2$	96

NOMENCLATURE

a_1, a_2	non-dimensional functions of Pr and Gr^*_R
Cp	specific heat, J/kg K
D	diameter, m
E	energy integral, J/m K
Fo_R	Fourier number = $\alpha t/R^2$
F_c	centrifugal force, N
F_{BH}	buoyancy force, N
f	non-dimensional stream function of ϕ, η
g	gravitational acceleration, m/s^2
$\bar{g}$	gravity force, N
Gr_R	Grashof number = $\frac{g\beta\Delta TR^3}{\nu^2}$
Gr^*_R	modified Grashof number = $\frac{g\beta qR^4}{k\nu^2}$.
h	heat transfer coefficient, W/m^2K
H	heat function, W/m^2K
$\bar{H}$	rate of change of bulk temperature with time, K/s
i,j	indices in a grid system
k	thermal conductivity, W/m K
L(Y)	associated cord length, non-dimensional
$L(\phi)$	width of stratified layer at an angle of ϕ,m
m	power variation of boundary layer velocity
$\dot{m}_{b\ell}$	boundary layer mass flow rate, kg/s
$\dot{m}_{s\ell}$	rate of increase of mass in stratified layer, kg/s

n	power variation of boundary layer thickness
Nu	Nusselt number = $\frac{hx}{k}$
$\overline{Nu}$	mean Nusselt number = $\int_0^{\pi} \frac{q}{\Delta T} \frac{x}{k} dx/L$, $(L = 2\pi R)$
P	pressure, N/m^2
Pr	Prandtl number = ν/α
q	wall heat flux, W/m^2
R	radius, m
r	polar coordinate on r,ϕ plane
T_∞	temperature, K
T_s	interface temperature, K
T	ambient temperature, K
T^*	dimensionless stratification profile
t	time, s
ΔT	reference temperature difference, K
u	tangential velocity along the wall, m/s
u_∞	reference velocity ($u_\infty = \sqrt{g\beta qR^2/k}$ or $u_\infty = \sqrt{g\beta\Delta TR}$)
$U = \frac{u}{u_\infty}$	non-dimensional velocity in Cartesian coordinates
v	radial velocity, m/s
$V = \frac{v}{u_\infty}$	non-dimensional velocity in Cartesian coordinates
$\bar{V}$	velocity vector with components u,v
W	non-dimensional vorticity
w	stratification angle
w_0	relaxation coefficient
$x = R$	coordinate along the wall of the cylinder, m
x_c	Cartesian coordinate, m

y	coordinate normal to the curved surface, m
y_c	Cartesian coordinate, m
X,Y	non-dimensional Cartesian coordinates
Z^*	thickness of stratified layer, m
Z	coordinate in the direction of stratification growth, dimensionless

Greek letters

A	non-dimensional temperature external to the boundary
α	thermal diffusivity, m^2/s
α_s	fill angle, rad
$\alpha_1, \alpha_2, \alpha_3, \alpha_4$	constants
β	coefficient of thermal expansion, 1/K
γ	non-dimensional parameter in stratified layer (coordinate)
Δ^+	non-dimensional boundary layer thickness = δ/R
ζ, η	non-dimensional coordinates in transformed domain
$\bar{\eta}$	non-dimensional coordinate normal to the curved surface
θ	non-dimensional temperature
λ	function of Prandtl number
ν	kinematic viscosity, m^2/s
Π	function of Prandtl or modified Grashof number (Π_L = laminar, Π_T = turbulent)
ρ	mass density, kg/m^3
τ_ω	wall shear stress, N/m^2
τ^+	non-dimensional time = $\frac{\nu}{R^2}\sqrt{Gr_R}$ or $\frac{\nu}{R^2}\sqrt{Gr^*_R}$

ϕ	angle measured from the bottom of the cylinder, rads
Φ	angle of incidence of the wall heat flux vector, rads
ψ	non-dimensional stream function
$\tilde{\phi}$	stability limit
δ	boundary layer thickness, m
δ_{ℓ}	laminar sublayer thickness, m
Ω	boundary layer velocity scale, m/s
Ω^{+}	non-dimensional boundary layer velocity scale ($= \Omega/\alpha/R$)
Ω^{*}	non-dimensional boundary layer velocity scale ($=\Omega/u_{\infty}$ where $u_{\infty} = (g\beta qR^{2}/k)^{1/2}$)
μ	dynamic viscosity, kg.m/s
$\Delta\zeta$	grid size, dimensionless
$\forall$	volume of stratified layer, m^{3}

CHAPTER 1

1.1 Objectives

The present study deals with the mechanism of free convective heat transfer inside a circumferentially heated, partially filled horizontal cylinder. The objective is to be able to predict the temperature-time history of the vessel and its contents in the liquid region, hence determining the rate of increase of pressure in the vapor.

The thermodynamic fluid state between the liquid and its vapor assumes an adiabatic interface in the first instance. The problem in its simplified form, consists of a partially filled vessel and is a typical example for natural convection in enclosed spaces, as shown in Fig. 1. As will be discussed now and in the following chapters, all previous work on natural convection in enclosed spaces has considered rectangular cavities, vertical cylinders or completely filled horizontal cylinders. The characteristics of the flow in a partially filled horizontal cylinder are however completely different. These differences will be made clear later when the results of a computer simulation are presented in Chapter IV.

The present analysis has its applications in the early stages of heat transfer to a derailed tank car loaded with

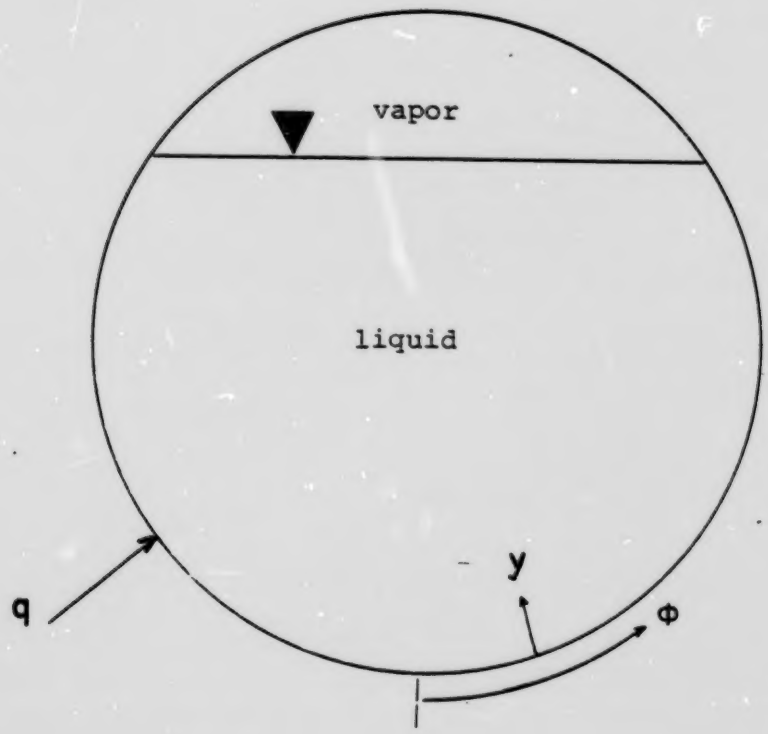

FIGURE 1. Partially filled horizontal cylinder heated from the side.

a cryogenic liquid and engulfed in flames. Such a fire most probably will start due to the presence of hot spots (such as a hot brake component) which act as igniters to the leaking gas from a ruptured tank car. The torch fire resulting in this manner, soon converts to a pool fire due to the spreading of leaking vapor or liquid around a neighbouring car whose lading temperature increases very rapidly as a result of this intensive radiation load. More information on this type of accident may be found in [1].

The early stages of heat transfer in such a vessel are by means of free convection. Since the fluid is confined in a vessel, the present problem then falls under the category of the so called area of "Natural Convection in Enclosures". This topic has received only a little attention relative to the problems in external free convection where direct applications abound, in oceanography, in meteorology, flow over heated surfaces, in manufacturing and processing, flight, shipping and energy systems.

In external problems, Prandtl's boundary layer theory is directly applicable and the complete equations of motion are reduced to the so called "boundary layer equations", where it is presumed that the boundary layer flow does not affect the external medium.

Contrary to the above flows, in internal convection

problems the boundary layer affects the surrounding fluid, therefore coupling the two regions. This coupling constitutes the main source of difficulty in obtaining analytical solutions to enclosure problems.

The problem at hand besides this possesses difficulties arising due to the partial filling. That is, the boundaries surrounding the liquid are not aligned with the coordinate system as in the case of a rectangular enclosure or a completely filled horizontal cylinder where Cartesian or polar coordinates can be used with ease (Fig. 1). In Chapter IV, however, a method is introduced to overcome this difficulty and similar ones that can be faced in practical applications.

The pioneering works concerning the internal problem are discussed in detail by [2] and [3] most of them dealing with rectangular geometries. These works and the more recent ones can be divided into three categories:

(a) Exact solutions to special cases. For example [2] has solved the case of a non-uniformly heated horizontal cylinder for a large Prandtl number and a Grashof number of unity.

(b) Numerical solutions. The finite difference solution of [4] for a horizontal cylinder.

(c) Experimental works. [5] and [6] have performed experiments where the sides of a horizontal cylinder were subjected to constant (in time) and non-uniform (on the

circumference) temperatures. In Chapter IV, the results of these two experiments will be compared with the present study as special cases since the former, [5] involves a low Prandtl (Pr = 0.72) and a high Grashof ($Gr = 10^7 - 4.5 \times 10^7$) number fluid while the latter, [6] has worked with a high Prandtl (Pr = 18600 - 19950) and low Grashof number (Gr = 1.1 - 2.4) fluid.

All of the studies mentioned above are related to the horizontal cylinder configuration. Those that are related to rectangular enclosures are omitted in the present discussion.

The following qualitative descriptions are due to the experiments carried out with a 380 mm diameter stainless steel tank heated uniformly (excluding a small portion of approximately 30° chord angle at the top) whose ends are covered with plexiglass walls permitting clear visualization and video recording. The details of instrumentation control hardware and software along with the experimental procedure are discussed in [11].

1.2 Physical Phenomena

When the walls of the horizontal tank are suddenly exposed to uniform heating, heat is transferred to the fluid core mainly by conduction. After a short time delay, buoyancy forces overcome gravitational forces and the fluid adjacent to walls rises along the walls, up to the free

surface, as depicted in Fig. 2. The heated fluid spreads towards the center as it reaches the surface and gradually forms a distinct warm layer in which a positive temperature gradient exists with a maximum at the interface. The flow inside the cylinder is recirculating in nature, but the magnitudes of the velocities inside the bulk of the liquid are essentially very much smaller than the boundary layer velocities. The stratification developed in this form is stable and the shape of the temperature profile in the vertical direction does not change significantly as time progresses, although the circulatory motion accelerates. The pressure in the vapor space is at a saturation condition consistent with the liquid interface temperature. That is, the interface temperature controls the pressure in the vapor space. The determination of time dependent stratification is, therefore, of considerable importance.

Another observation made from the experiments is that of an unstable region at the cylinder bottom. In this region, the heat transfer mechanism is similar to the case where a horizontal or nearly horizontal heated plate faces upwards. In this unstable region mixing between heated and core fluid occurs contributing to the increase of bulk temperature. It is necessary, therefore, to predict the initiation of the stable wall boundary layer after this region and modify the integral analysis accordingly.

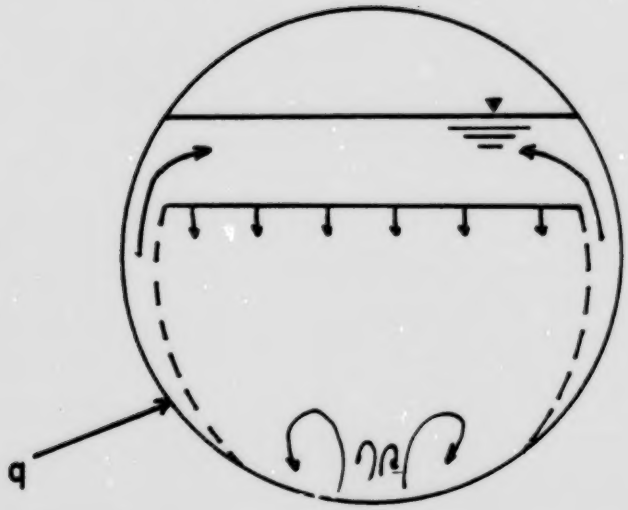

FIGURE 2. Physical picture.

In summary, the following can be deduced from the above description:

(a) There exists a thin boundary layer where the velocities are much higher than the downward core velocities.

(b) The fluid layers in the stratified region are isothermal in a horizontal direction.

(c) Furthermore, relying on experimental data, for moderate heat fluxes at the order of 20 kw/m^2, it can be stated that the core region below the stratified layer is in a quasi isothermal state. That is, the spatial temperature distribution in the core is uniform for all times but the core temperature can increase as time progresses. In Fig. 3 the region below the dashed lines is indicating the presence of isothermal conditions in the core with almost vertical profiles (note that each profile is at a different time level), therefore justifying this assumption.

Item (a) stated above automatically uncouples the internal core from the boundary layer flow and allows a treatment similar to an external boundary layer problem while (b) permits the use of a single temperature profile in the stratiiied layer in the vertical direction. In (c) it is suggested that influence of external stratification can be neglected at the early stages of heating such as warm liquid injection into the core from the boundary layer. The effects of this case are determinec in a separate analysis and examined for various degrees of

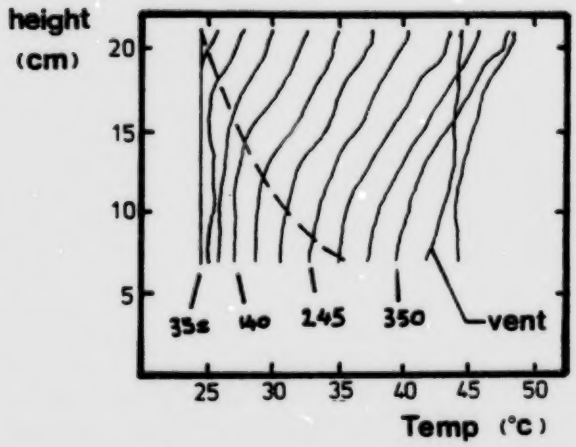

FIGURE 3. Transient development of vertical temperature profiles for q=20 kw/sq.m,92% fill,without EXPLOSAFE.

stratification after presenting an integral analysis.

1.3 Mathematical Model

In this study two approximate approaches are presented due to the difficulties stated above. It is obvious that a series of assumptions are inevitable if one is to obtain any solution since the governing equations are highly nonlinear and coupled.

The first of these two solution techniques is an integral method which presumes uncoupling (in the sense of flow dynamics not in the equations) between the boundary layer and the external flows. The second and more involved one is the numerical integration of the full equations of motion where more information about the total flow regime and heat transfer can be obtained. The disadvantages and advantages of these two techniques will become clear later in Chapters III and IV.

It is now appropriate to state the general problem of natural convection along with the most commonly utilized assumptions necessary for realistic solutions:

Momentum

$$\rho \frac{D\bar{V}}{Dt} = -\bar{\nabla}p + \mu \nabla^2 \bar{V} + \bar{g} \left[\rho - \rho\beta (T-T_\infty)\right]^* \qquad (1.1)$$

---

*The substantial derivative operator $\frac{D}{Dt}$ is defined as $\frac{Df}{Dt} = \frac{\partial f}{\partial t} + (\bar{V}\cdot\bar{\nabla}f)$.

Energy

$$\rho C_p \frac{DT}{Dt} = k\nabla^2 T \qquad (1.2)$$

Continuity

$$\bar{\nabla}\cdot\bar{V} = 0 \qquad (1.3)$$

In the above equations it has been assumed that:

(1) the fluid is Newtonian;

(2) the fluid properties are constant in time and space; and

(3) the flow is incompressible.

For free convective flows, it is further assumed that:

(4) the external pressure is constant;

(5) viscous dissipation is negligible;

(6) the density variation is neglected except for its effect in the body force term. (Usually, the density is expanded in Taylor series about a reference point. For a valid expansion, $\beta(T-T_\infty)<<1$ must be satisfied. See [3] pp. 19-21, "Boussinesq Approximation"); and finally

(7) the dynamic pressure is negligible, hence considering only the static one, it can be written that $\bar{\nabla}p = \rho\bar{g}$.

With these assumptions, eqns. (1.1) to (1.3) reduce, for two dimensional flow to:

$$\frac{\partial u}{\partial x_c} + \frac{\partial v}{\partial y_c} = 0$$

$$\frac{\partial u}{\partial t} + u\frac{\partial u}{\partial x_c} + v\frac{\partial u}{\partial y_c} = -\beta(T-T_\infty)g_{x_c} + \nu\left(\frac{\partial^2 u}{\partial x_c^2} + \frac{\partial^2 u}{\partial y_c^2}\right) \qquad (1.4)$$

$$\frac{\partial v}{\partial t} + u\frac{\partial v}{\partial x_c} + v\frac{\partial v}{\partial y_c} = -\beta(T-T_\infty)g_{y_c} + \nu\left(\frac{\partial^2 v}{\partial x_c^2} + \frac{\partial^2 v}{\partial y_c^2}\right) \qquad (1.5)$$

$$\frac{\partial T}{\partial t} + u\frac{\partial T}{\partial x_c} + v\frac{\partial T}{\partial y_c} = \alpha\left(\frac{\partial^2 T}{\partial x_c^2} + \frac{\partial^2 T}{\partial y_c^2}\right) \qquad (1.6)$$

These equations can be found in standard texts where they are treated in more detail ([7], [8]).

It should be noted that these equations are in the same form for a horizontal cylinder if we let $x = R\phi$ and $y = -r$ as in [9].

At this point one can now go to a complete numerical integration of eqns. (1.4) to (1.6) or further simplify them using boundary layer assumptions.

The former approach will be discussed in Chapter IV where a new technique of orthogonal coordinate transformation is introduced. The boundary layer simplification is going to be stated now and developed in Chapters II and III.

The validity limits of the assumptions for boundary layers are discussed elsewhere in detail ([10], pp. 127-129) and will only be stated here in a summarized form:

$$y/x << 1,\ v/u << 1,\ \frac{\partial^2 u}{\partial x^2} << \frac{\partial^2 u}{\partial y^2} \tag{1.7}$$

Utilizing the above, eqns. (1.4) to (1.6) assume the form

$$\frac{\partial u}{\partial x} + \frac{\partial v}{\partial y} = 0 \tag{1.8}$$

$$\frac{\partial u}{\partial t} + u\frac{\partial u}{\partial x} + v\frac{\partial u}{\partial y} = \nu\frac{\partial^2 u}{\partial y^2} + g\beta(T-T_\infty)\sin\phi \tag{1.9}$$

$$\bar{H} + \frac{\partial T}{\partial t} + u\frac{\partial T}{\partial x} + v\frac{\partial T}{\partial y} = \alpha\frac{\partial^2 T}{\partial y^2} \tag{1.10}$$

where $\bar{H}$ is given by

$$\bar{H} = \frac{dT_\infty}{dt} \tag{1.11}$$

which is the effect of increasing bulk or surrounding temperature due to heating. It has been shown, [9], that this effect is negligible if $\delta << R$, which is a good assumption for large diameter cylinders since δ is very thin.

1.4 Possible Solutions of the Governing Equations of Motion

Eqns. (1.4) to (1.6) and (1.8) to (1.9) are two possible models available to predict the flow behaviour in natural convection problems. Eqns. (1.4) to (1.6) admit exact solutions under very special cases such as large Prandtl and low Grashof numbers which essentially uncouple the energy and momentum equations. In the absence of such a simplification, one has to resort to numerical integration

since it becomes necessary to solve all the equations in coupled form.

On the other hand, eqns. (1.8) to (1.10) are simpler and can be solved either with integral (the well known Karman-Pohlhausen Integral Momentum Method) or asymptotic methods. In cases where the sin ϕ term does not appear in the body force (i.e. a flat surface), a similarity transformation becomes possible which reduces the boundary layer equations to nonlinear third order coupled ordinary differential equations. These permit reliable results as long as the assumptions of the boundary layer are valid (see [10], p. 316 or [3], p. 49 for a detailed discussion). For the present problem an integral approach is justified at least for the early stages of heating to obtain fairly good information about the heat transfer mechanism inside the vessel.

CHAPTER II

INTEGRAL ANALYSIS

2.1 Introduction

The integral method of analysis was originally developed by T. Karman for forced flows. It may also be employed to solve problems involving buoyancy induced motion. A discussion of the method as applied to forced flows can be found in [10], (p. 206), whereas those that are related to natural convective flows are discussed in [3]. The technique gives good approximations to boundary layer problems when an exact solution is difficult or impossible to obtain.

The principle of the method is simple such that one only makes a force balance in an integrated sense, instead of a differential approach. If the flow is turbulent, it is customary to use empirical relations for the temperature and velocity profiles satisfying the imposed or natural boundary conditions in the cross stream direction. The resulting equilibrium equations will then only be functions of x, that is the downstream coordinate. If an empirical relation is given for the wall shear stress, then the original nonlinear equations of boundary layer flows will reduce to first order nonlinear, single parameter equations

and can be solved by conventional methods such as the powerlaw variation technique.

If the flow is laminar there is no need for an empirical velocity or temperature profile and it is sufficient to use parabolic profiles which satisfy the two boundary conditions at the wall and at the edge of the boundary layer. The shear stress can also be evaluated with its usual definition ($\tau_\omega = \mu \frac{\partial u}{\partial y}$) evaluated at the wall using the profile for velocity.

2.2 Analysis

In what follows an outline of the integral analysis used in this work will be given. The method is straightforward and semi-empirical in the sense that the shape of the similarity profiles for tangential velocity and temperature are assumed to be known.

Integration of equations (1.9) and (1.10) in the direction of the y coordinate and use of eqn. (1.8) results in:

Momentum

$$\frac{\partial}{\partial x}\int_0^\delta u^2 dy = \int_0^\delta \beta g(T-T_\infty)\sin\phi\, dy - \frac{\tau_\omega}{\rho} \qquad (2.1)$$

Energy

$$\frac{\partial}{\partial x}\int_0^\delta u(T-T_\infty)dy = -\alpha \frac{\partial T}{\partial y}\bigg|_{y=0} \qquad (2.2)$$

subject to the boundary conditions.

$$u = \frac{\partial u}{\partial y} = \frac{\partial T}{\partial y} = 0 \quad \text{at } y = \delta$$
$$u = 0, \; -k\frac{\partial T}{\partial y} = q \quad \text{at } y = 0 \tag{2.3}$$

The following profiles for laminar flow satisfy the above conditions:

$$T - T_\infty = \frac{q\delta}{2k}\left(1 - \frac{y}{\delta}\right)^2 \tag{2.4}$$

$$\frac{u}{\Omega} = \frac{y}{\delta}\left(1 - \frac{y}{\delta}\right)^2 \tag{2.5}$$

Substitution of eqns. (2.4) and (2.5) in eqns. (2.1) and (2.2) integration results in a first order ordinary differential equation in x. This can be solved by assuming a power law variation for Ω and δ in the form:

$$\Omega = a_1 x^{\bar{m}}, \; \delta = a_2 x^n \tag{2.6}$$

where Ω and δ are the velocity and boundary layer scales respectively. Solving for a_1 and a_2 results in:

$$\Delta^+ = 3.1\left[\frac{1/Pr^2 \cdot 1.25/Pr}{Gr^*_R \sin\phi}\right]^{1/5} \phi^{1/5} \tag{2.7}$$

$$\Omega^+ = 6.23\left[\frac{1/Pr^2 + 1.25/Pr}{Gr^*_R \sin\phi}\right]^{-2/5} \phi^{3/5} \tag{2.8}$$

It should be noted that in the derivation of eqns. (2.7)

and (2.8) the variation in the buoyancy term due to sin in eqn. (2.1) is neglected. One of the important conclusions of this study however, is that the above equations are in fact an excellent representation for the boundary layer flow along a curved surface since they give almost identical solution to the exact solution of eqns. (2.1) and (2.2) as will be outlined in section 3. Eqns. (2.7) and (2.8) will be used throughout the integral analysis here due to their closed and convenient form; the exact solution can only be expressed in a series form. Another point to be considered is that the power variations of (1/5) and (3/5) of the ϕ term in eqns. (2.7) and (2.8) agree with other studies for the constant wall heat flux such as that in [12] where a transient free convection problem for the flat plate is considered using the method of characteristics.

The application of the integral technique to turbulent free convection boundary layer flows was first seen in the work of [13].

The empirical velocity and temperature profiles used by them are:

$$\frac{u}{\Omega} = \left(\frac{y}{\delta}\right)^{1/7}\left(1-\frac{y}{\delta}\right)^{4} \tag{2.9}$$

$$\frac{T-T_\infty}{\bar{T}-T_\infty} = \left[1-\left(\frac{y}{\delta}\right)^{1/7}\right]. \tag{2.10}$$

Since eqn. (2.10) yields an infinite gradient at $y = 0$, it is not possible to impose the heat flux boundary condition

at the wall. A linear temperature profile in the laminar sublayer is therefore assumed to have a thickness [14],

$$\delta_\ell = 15\nu\sqrt{\delta/\tau_\omega} \tag{2.11}$$

where
$$\tau_\omega = 0.0225\rho\ \Omega^2\left(\frac{\nu}{\Omega\delta}\right)^{1/4}. \tag{2.12}$$

The same form for τ_ω has been used by [13], [15], [16] and [17] in related problems. Eqn. (2.10) can now be rewritten as follows:

$$T-T_\infty = 44\ \frac{q}{\rho C_p}\left(\frac{\delta}{\nu\Omega^3}\right)^{1/4}\left[1-\left(\frac{y}{\delta}\right)^{1/7}\right] \tag{2.13}$$

Using a power law variation as in eqn. (2.7), the following equations for turbulent boundary layer thickness and velocity scales are obtained:

$$\Delta^+ = 0.525\left(\frac{Pr}{Gr^*_R \sin\phi}\right)^{1/4}\phi^{5/7} \tag{2.14}$$

$$\Omega^+ = 3.84\left(\frac{Pr}{Gr^*_R \sin\phi}\right)^{-5/14}\phi^{3/7} \tag{2.15}$$

The powers (5/7) and (3/7) in eqns. (2.14) and (2.15) are in agreement with the turbulent expressions of [15] and [16] for related problems.

In the following section the approximation introduced due to the neglected sin ϕ variation in the buoyancy term

will be discussed.

2.3 An Exact Solution of the Integral Equations of Motion

Using laminar profiles for example, the integrated forms of eqns. (2.1) and (2.2) in non-dimensional form are:

$$\frac{d}{d\phi}\left(\Delta^{+}\Omega^{*^2}\right) = 17.5\,\Delta^{+^2}\sin\phi - \frac{105}{\sqrt{Gr^{*}_{R}}}\,\frac{\Omega^{*}}{\Delta^{+}} \tag{2.16}$$

$$\frac{d}{d\phi}\left(\Delta^{+^2}\Omega^{*}\right) = \frac{60}{Pr\sqrt{Gr^{*}_{R}}} \tag{2.17}$$

where $\Omega^{*} = u/u_{\infty}$, $u_{\infty} = \sqrt{g\beta q R^2/k}$.

These two sets of equations have been solved until now by using power law relations such as for the vertical flat plate where the sin ϕ term is absent in the body force. The method outlined below can be applied to both flows, that is either flat or curved, and there is no need for a power law assumption.

Introducing the variable

$$\Gamma = \Delta^{+^2}\Omega^{*} \tag{2.18}$$

equation (2.17) can be integrated to give

$$\Gamma(\phi) = \frac{60\,\phi}{Pr\sqrt{Gr^{*}_{R}}}\,. \tag{2.19}$$

Rewriting eqn. (2.16) using eqn. (2.19) and simplifying results in

$$\frac{d\Delta^+}{d\phi} - \frac{\Delta^+}{\phi}\left(\frac{7}{12}\,Pr + \frac{2}{3}\right) = -Gr^*_R Pr^2 \left(\frac{17.5}{10800}\right)\frac{\Delta^{+6}}{\phi^2}\sin\phi \qquad (2.20)$$

Eqn. (2.20) is of the form

$$\Delta^{+'} + P(\phi)\Delta^+ = Q(\phi)\Delta^{+n} \qquad (2.21)$$

P and Q are functions of ϕ. This equation is in the form of the famous Bernouilli's equation. The general solution of which is given in any handbook of mathematics (see [18] for instance) as

$$\Delta^{+1-n} = \exp[(n-1)\int P(\phi)d\phi]\{(1-n)\int Q(\phi)\exp[(1-n)\int P(\phi)d\phi]d\phi + C\} \qquad (2.22)$$

where in this case

$$P(\phi) = -\frac{1}{\phi}\left(\frac{7}{12}\,Pr + \frac{2}{3}\right)$$

$$Q(\phi) = -Gr^*_R Pr^2 \left(\frac{17.5}{10800}\right)\frac{\sin\phi}{\phi^2} \qquad (2.23)$$

and $n = 6$, for $\phi > 0$.

The final result can now be shown to be

$$\Delta^+ = \left[\frac{Gr_R^* Pr^2}{123}\left\{\frac{1}{\lambda+2} - \frac{\phi^2}{3!(\lambda+4)} + \frac{\phi^4}{5!(\lambda+6)} + \ldots\right\}\right]^{-1/5} \qquad (2.24)$$

where $\lambda = \frac{35}{12} Pr + 1.33$.

Using eqns. (2.18) and (2.19),

$$\Omega^* = \frac{8.75\,\phi}{(Pr^2 Gr_R^*)^{1/10}}\left\{\frac{1}{\lambda+2} - \frac{\phi^2}{3!(\lambda+4)} + \frac{\phi^4}{5!(\lambda+6)} + \ldots\right\}^{2/5} \qquad (2.25)$$

The interval of convergence of these series is infinite therefore the given forms are valid for all positions along the cylinder since ratio test will show that this is true for all ϕ.

The solutions given by eqns. (2.7) and (2.8) can now be compared to the exact solutions. Rewriting eqn. (2.8) in the new non-dimensional form used here results in,

$$\Omega^* = \frac{6.23}{(PrGr_R^*)^{1/10}} \sin^{2/5}\phi \left(\frac{1}{Pr^2} + \frac{1.25}{Pr}\right)^{-2/5} \phi^{3/5} \qquad (2.26)$$

Fig. 4.a plots $\Omega^* \cdot (Gr_R^*)^{1/10}$ versus ϕ as given in eqns. (2.25) and (2.26); very close agreement can be observed. Similarly eqns. (2.7) and (2.24) show very close agreement in Fig. 4.b for $\Delta^+(\phi)$.

The above proves that eqns. (2.7) and (2.8) are as good as the exact solution and can be used with confidence at least to $\phi \leq 3.0$.

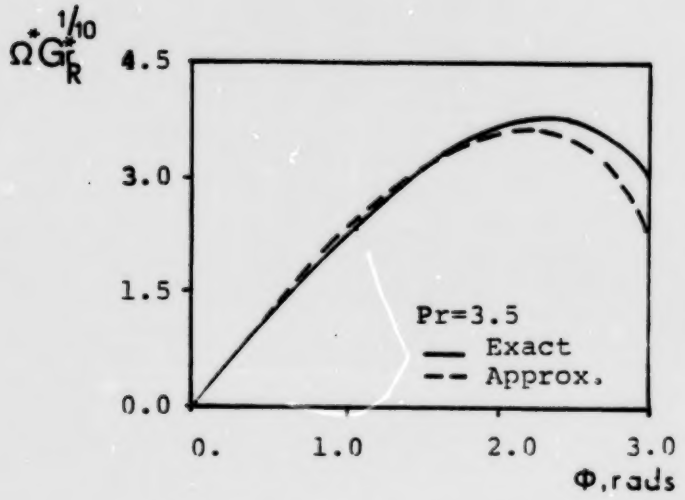

FIGURE 4.a Comparison of velocity scales.

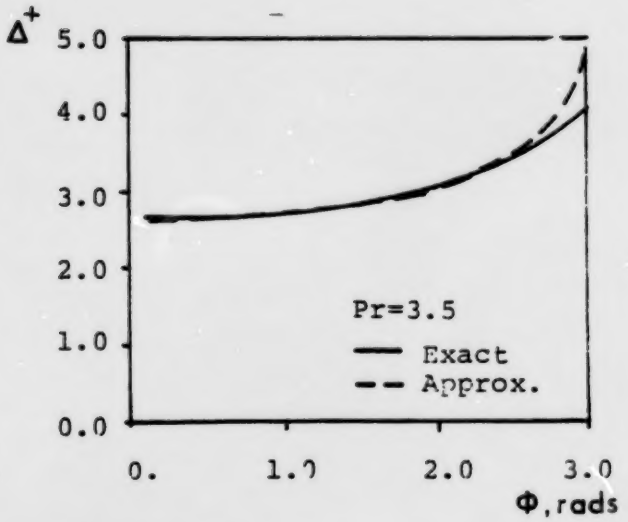

FIGURE 4.b Boundary layer growth.

Further comparison with respect to mean Nusselt number can be made. It can be shown that this is given by eqn. (2.27) for the approximate solutions of section 2.2.

$$\overline{Nu} = \frac{1}{L_c} Gr_R^{*1/5} \frac{1}{3.1\left(\frac{1}{Pr^2} + \frac{1.25}{Pr^2}\right)^{1/5}} \int_0^{\pi} 4/5 \sin^{1/5}\phi \, d\phi \quad (2.27)$$

and for the exact solution of this section by

$$\overline{Nu} = \frac{1}{L_c} \left(\frac{123}{Pr^2}\right)^{1/5} Gr_R^{*1/5} \int_0^{\pi} \left(\frac{\phi^5}{\lambda+2} - \frac{\phi^7}{3!(\lambda+4)} + \frac{\phi^9}{5!(\lambda+6)} + \ldots\right)^{1/5} d\phi \quad (2.28)$$

where $L_c = 2L/R$ is a characteristic length.
Eqns. (2.27), and (2.28) are plotted versus the Prandtl number in Fig. 4.c and again the results are in good agreement over a wide range of Prandtl number.

It is possible to compare these local Nusselt numbers with that of a perturbation solution given by [19].
In that work free convection heat transfer from a horizontal cylinder with a variable wall temperature is considered. (Figs. 5.a and 5.b). Two comparisons are made at Pr = 1 and Pr = 0.7 since those are the only ones reported in [19]. Agreement with the present exact solution is good but the approximate solution, which does not consider the variation of body force with sin ϕ term deviates for $\phi > 135°$. This does not however limit the applicability of eqns. (2.7) and (2.8) since in most partial fillings, the region of

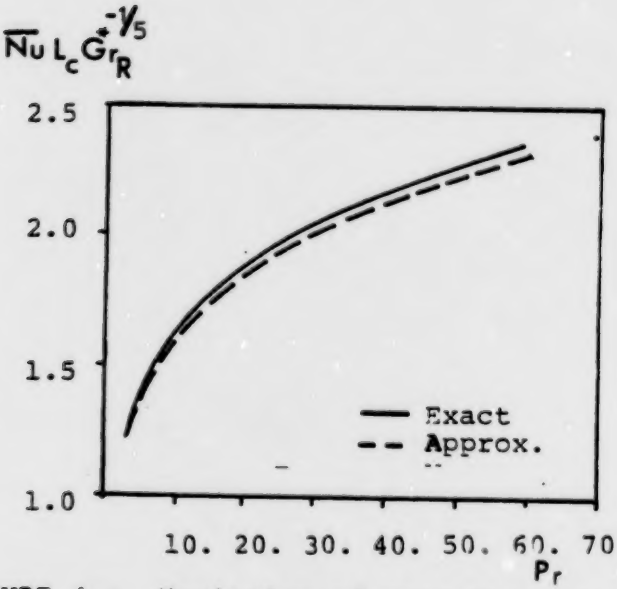

FIGURE 4.c Variation of mean Nusselt number with Prandtl number.

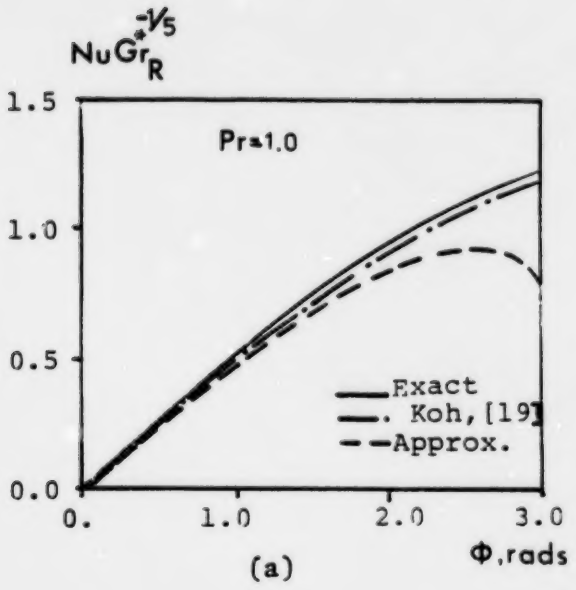

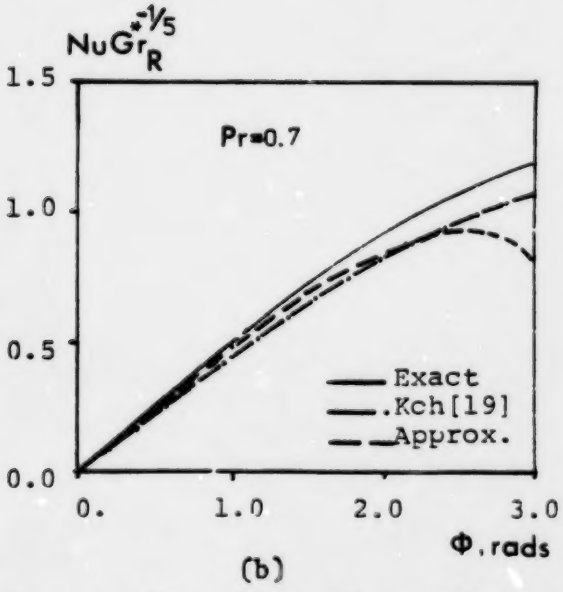

FIGURE 5 Local variation of Nusselt number with position along the wall, (a) Pr=1.0, (b) Pr=0.7 .

interest does not exceed this value.

In the above comparison the local variation of Nusselt number in its rearranged form as given in [19] is

$$\frac{Nu}{Gr_R^{*1/5}} = \frac{\phi}{1.9963 + .04361\phi^2 + 0.015\phi^4} \qquad (2.29.a)$$

(for Pr = 1)

The exact solution of this section results in

$$\frac{Nu}{Gr_R^{*1/5}} = \frac{\phi}{1.309}\left[\frac{1}{\lambda+2} - \frac{\phi^2}{3!(\lambda+4)} + \ldots\right]^{+1/5} \qquad (2.29.b)$$

with the approximate form as

$$\frac{Nu}{Gr_R^{*1/5}} = \frac{\phi^{4/5}}{1.823}\sin^{1/5}\phi \qquad (2.29.c)$$

when Pr = 1.0.

The solutions given above may also be expressed in terms of Pr number and with this respect are more general than those given by [19]. To obtain the variation in $\overline{Nu}$ with respect to Pr, [19] must solve the perturbation equations for each value of Prandtl number whereas in this case they are in closed form.

In the next chapter a thermal stratification model is outlined which utilizes the boundary layer expressions derived in this chapter.

CHAPTER III

A THERMAL STRATIFICATION MODEL

3.1 Introduction

In general there have been three approaches to stratification problems in closed containers: a) integral method, b) numerical integration of eqns. (1.4) to (1.6) and c) experimental studies. These methods are now going to be discussed individually.

a) By assuming that boundary layer flow is independent of core motion, integral techniques have been extensively used and the results are in reasonable agreement with experimental data. The early works in this direction originated from research on cryogenic fuel stratification in rocket propellant tanks. [20] has studied a pressurized container with side wall heating where the heat diffusing directly into the core region from the wall was determined by comparison with experimental data. He reports results for a case where all the heat incident on the vessel is carried directly into the thermal layer. The analyses given in [21] and [22] are also for cryogenic stratification in vertical tanks, however they assume isothermal wall temperatures which can be justified for low heat flux levels. [21] has good agreement for $q = 8\ kw/m^2$, however appreciable deviations occur for higher heat fluxes. On the other hand

[22] did not report on the magnitude of the heat flux. The integral equations of motion have been solved numerically in their quasi-steady state form with the presence of an axial temperature gradient in the core region for vertical tanks [15, 16, 17]. The results of [17] are for very low heatings (maximum heating was $q = 1.6$ kw/m^2) and most probably the effects of turbulent mixing were absent. They report better agreement with data compared to [15] since the latter overpredicted the interface temperatures most probably due to turbulent eddy diffusion. In general however, their results indicate good predictions in the overall sense.

[15] and [17] have reported on the thinning of the momentum boundary layer thickness and [16] has noted its effect on the delay of transition to turbulence. The latter result is expected since the net effect of the external stratification is to decrease velocities in the boundary layer and damp out any disturbances that may otherwise amplify if the flow accelerates. These points will be discussed later in the following sections.

b) The second approach has been the complete integration of the equations of motion. A study by [23] considers a case where a vertical enclosure is heated and cooled on the opposite sides. They used Rayleigh numbers from 10^4 to 10^6 and aspect ratios varying from 1 to 18 where the aspect

ratio is defined as height to width ratio in two dimensional studies. For smaller aspect ratios their numerical results show that the isotherms in the core region are nearly horizontal but that the core is stratified. Similar result can be observed in the numerical computations of [24] where uniform side wall heating was considered in a rectangular cavity.

c) The third approach is the experimental one and a well known observation is due to [25] who, in detail have studied the stratification phenomena in rectangular enclosures, heated from the sides and the bottom. An important conclusion of this work is the translation of vertical temperature profiles in time after complete stratification (for $Ra^{*} = 10^{10}$). Another result is the flatness of the base of the stratified layer and its clear distinction from the unstratified region. These results confirm the assumptions necessary for analysis in the next section, where a distinct stratified region is presumed. In [26] experiments with a vertical cylindrical tank showed that bottom heating was mainly responsible for the core temperature increase and in the case of side wall heating only, the tank stratified with less increase in the bulk temperature (shown in their Fig. 1). The core here was perfectly isothermal and the progress of thermal layer downwards could be observed through the progression of vertical temperature profiles with time.

3.2 A Model for Thermal Stratification

In what follows, an outline of the stratification analysis is given.

The rate of mass flow in the boundary layer should be equal to the rate of increase of mass in the stratified layer, that is, $\dot{m}_{b\ell} = \dot{m}_{s\ell}$ where

$$\dot{m}_{b\ell} = \int_0^{\delta} \rho u dy \tag{3.1}$$

and

$$\dot{m}_{s\ell} = \rho \frac{d\forall}{dt} \tag{3.2}$$

$\forall(\phi) = R^2[\pi - (\phi + \alpha_s) + 1/2(\sin 2\phi + \sin 2\alpha_s)]$ in m^3/m expresses the volume of stratified layer as a function of α_s, the stratification angle measured from $\phi = 180°$.

Substituting eqn. (2.5) (or eqn. (2.9) for turbulent flow) in eqn. (3.1) and equating it to eqn. (3.2) results in

$$\int_{\pi-\omega}^{\pi-\alpha_s} \frac{\cos 2\phi - 1}{\phi^{.8} \sin^{.2}\phi} d\phi = 3.22\ Fo_R\ \Pi_L(Pr, Gr^*_R) \tag{3.3}$$

where

$$\Pi_L(Pr, Gr^*_R) = \left[\frac{1/Pr^2 + 1.25/Pr}{Gr^*_R}\right]^{-1/5}$$

and for turbulent flow

$$\int_{\pi-\omega}^{\pi-\alpha_s} \frac{\cos 2\phi - 1}{\phi^{8/7}\sin^{2/7}\phi}\, d\phi = 0.588\ Fo_R\ Pr\ \Pi_T(Pr, Gr_R^*) \quad (3.4)$$

where

$$\Pi_T(Pr, Gr_R^*) = (Pr/Gr_R^*)^{-2/7}$$

Eqns. (3.3) and (3.4) can be integrated for several values of Fo_R to obtain the growth of the thermal layer.

In order to determine the temperature variation, the total energy carried in the boundary layer will be equated to the integrated energy in the stratified region,

$$D(\pi-\alpha_s)\int_0^t q\,dt = \rho C_p \int_{\pi-\alpha_s}^{\pi-\omega} (T-T_\infty)L(\phi)d\phi = \rho C_p E \quad (3.5)$$

Experimental data for heat fluxes in the range of 0 - 40 kw/m^2 show that the temperature profile in the thermal layer has an inflection point, suggesting a third order polynomial shape. In addition there appears to be very little heat/mass transfer across the interface, thus

$$T^* = \frac{T-T_\infty}{T_s-T_\infty} = \alpha_1 + \alpha_2\gamma + \alpha_3\gamma^2 + \alpha_4\gamma^3 \quad (3.6)$$

subject to

$$T^* = 1 \quad \text{as} \quad \gamma \to 0$$

$$T^* = 0,\ \frac{dT^*}{d\gamma} \to 0 \quad \text{as} \quad \gamma \to 1 \quad \text{where} \quad \gamma = \frac{Z}{Z^*} \quad (3.7)$$

where $\alpha_1, \alpha_2, \alpha_3$ and α_4 are constants.

These result in

$$T^* = (2\gamma+1)(1-\gamma)^2 \qquad (3.8)$$

Using eqn. (3.8) in eqn. (3.5) yields

$$T_s - T_\infty = \frac{(\pi-\alpha_s)qt}{\rho C_p Z^* E} \qquad (3.9)$$

where E is the energy integral on the right hand side of eqn. (3.5).

Eqn. (3.3) (or eqn. (3.4) for the turbulent case) can now be used to predict the growth of the thermal layer while eqn. (3.9) predicts the interface temperature. These two equations are linked through the energy integral, E.

The horizontal cylinder geometry presents an additional boundary layer stability problem as will be discussed next.

3.3 Approximate Analysis of Hydrodynamic Stability of a Boundary Layer on a Concave Surface

The buoyancy induced instability in this problem is due mainly to the unbalanced components of vertical forces on a fluid element (in the integral sense) at the bottom of the cylinder. This can be best understood once the effective forces on a fluid element are considered (Fig. 6).

In addition to the body force and the force due to the

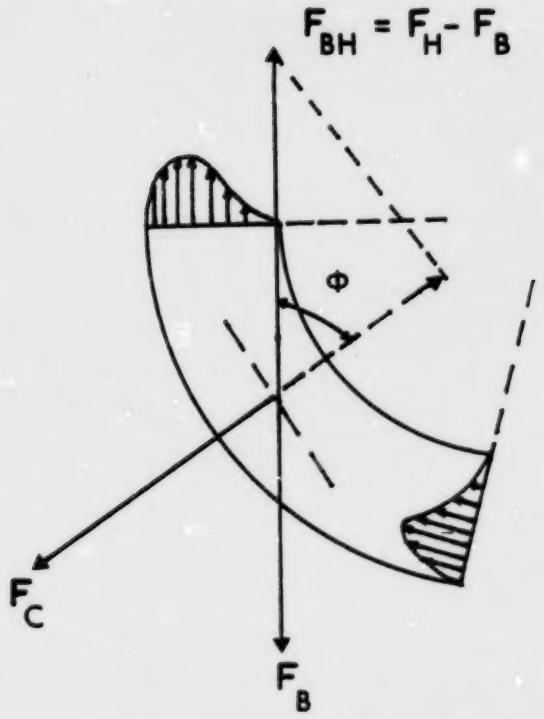

FIGURE 6. Normal forces on a fluid element. Tangential forces are not shown.

difference in hydrostatic pressure at the ends of the control volume, another force exists due to the presence of curvature. This is the centrifugal force, which acts in a direction opposite to the projection of the buoyancy force on an axis normal to the fluid element, thus preventing boundary layer separation. In the following analysis, any force perpendicular to the normal axis is not considered since it has no contribution in the stability of the element (e.g. the wall shear force); the algebraic sum of forces on this axis thus yields a sufficient criterion for stability. Projection of the body and the hydrostatic forces on the normal axis is, per unit length,

$$F_{BH} = \int_0^{\delta} g(\rho-\rho_\infty)\cos\phi\, dy = \int_0^{\delta} \beta g\rho(T-T_\infty)\cos\phi\, dy \qquad (3.10)$$

The centrifugal force is

$$F_c = \int_0^{\delta} \rho \frac{U^2}{R}\, dy \qquad (3.11)$$

For stability, the centrifugal force must be equal to or greater than the body and hydrostatic force. Integrating eqns. (3.10) and (3.11) using the appropriate laminar temperature and velocity profiles results in

$$\frac{221}{1+1.25Pr}\tilde{\phi}\tan\tilde{\phi} \geq 1 \qquad (3.12)$$

$\tilde{\eta} = .10075$ $\tilde{\phi} = 6°$

A similar analysis for turbulent flow gives

$$0.45\,\tilde{\phi}\tan\tilde{\phi} \geq 1 \qquad (3.13)$$

where the corresponding turbulent profiles are used. Strictly speaking, the above analysis is valid for Prandtl numbers at the order of unity since in the integral analysis, it was implicitly assumed that thermal and momentum boundary layers are equal in magnitude.* The same assumption can be seen in eqn. (3.10) and (3.11) (i.e. the integral limits are from 0 to δ) where only δ is used to indicate both thicknesses.

3.4 Complete Problem Description

The results of section 3 indicate that the free convective boundary layer starts at $\tilde{\phi}$ which is determined either by eqn. (3.12) or (3.13) depending on the flow conditions. This means that eqns. (3.3), (3.4) and (3.9) should be shifted in the ϕ direction as follows:

Eqn. (3.3) becomes

$$\int_{\pi-\omega}^{\pi-\alpha_s} \frac{\cos 2(\phi-\tilde{\phi}) - 1}{(\phi-\tilde{\phi})^{.8}\sin(\phi-\tilde{\phi})^{.2}}\, d\phi = 3.22\, Fo_R\, \Pi_L(Pr, Gr^*_R) \qquad (3.14)$$

*The estimated range of validity with respect to the Prandtl number is 0.7 - 8.0.

Eqn. (3.9) becomes

$$T_s - T_\infty = \frac{(\pi - \alpha_s - \tilde{\phi})qt}{C_p Z^* E} \qquad (3.15)$$

Eqn. (3.4) can also be rewritten similarly.

With this modification one can now determine the increase in the temperature of the core fluid as there is direct mixing in the region determined by eqns. (3.12) or (3.13). It should be noted however that this is a first order correction and a better limit may be obtained if eqns. (2.7) and (2.8) are rewritten as:

$$\Delta^+ = 3.1 \left[\frac{1/Pr^2 + 1.25/Pr}{Gr^*_R \sin(\phi - \tilde{\phi})}\right]^{1/5} (\phi - \tilde{\phi})^{1/5} \qquad (3.16)$$

$$\Omega^+ = 6.23 \left[\frac{1/Pr^2 + 1.25/Pr}{Gr^*_R \sin(\phi - \tilde{\phi})}\right]^{-2/5} (\phi - \tilde{\phi})^{3/5} \qquad (3.17)$$

In their shifted forms eqns. (2.4) and (2.5) can be modified using the above expressions and substituted in eqns. (3.10) and (3.11) thus obtaining a better limit. This process can be continued indefinitely to provide more accurate results.

3.5 Modification of Flow Properties for a Porous Boundary Layer

To deal with the physical situation in which EXPLOSAFE, an expanded aluminum foil heat transfer mesh, covers the inside walls of the tank, the following modifications to the fluid properties are made.

(a) The thermal conductivity is calculated based on the configuration of the aluminum mesh immersed in Freon 11 at stagnation conditions. A general methodology for this is given in [27] where the effective conductivity (solid and stagnant liquid) are given versus various void fractions at several solid to liquid conductivity ratios. The method used here is similar to that work. A typical EXPLOSAFE mesh unit cell was chosen and the transport of heat (by conduction) through this cell was extended to the entire medium. Simpler methods use the arithmetic mean of the contributions from each phase. The effective conductivity calculated for Freon 11 in the mentioned mesh is $k_{eff} \approx 0.164$ whereas the conductivity of Freon 11 itself is about $k_{R11} = 0.886$ W/m°C.

(b) The heat capacity and thermal expansion is unchanged. This can be shown to be true once the weighted averages are performed based on mass.

(c) The density of the mesh/fluid combination is the weighted average.

(d) The effective kinematic viscosity is 1.8 times

larger than that of Freon 11 based on the assumption of similarity between heat and momentum diffusion [10] which was also used in the integration of eqns. (2.1) and (2.2).

The proposed approach is very simple but a reasonable once since the EXPLOSAFE saturated fluid possesses a very low void fraction (~0.03). Its role is mainly to conduct heat away from the wall further into the core, essentially accelerating the stratification process since a larger amount of fluid is entrained in the boundary layer (due to the augmentation in the conductivity). Aside from these properties, the model represented by eqns. (3.14) and (3.15) remains unchanged.

The detailed methodology and example calculations are given in Appendix A.

3.6 Effects of External Stratification on the Boundary Layer

The effect of a positive temperature gradient on the free convection boundary layer has been studied by [28] where an isothermal flat plate was considered. The equations of motion were reduced to a set of ordinary differential equations through the definition of a stream function and series expansions for the flow variables (i.e. stream function and temperature).

The studies made so far are however limited to flat plates and in this section, the same phenomena will be

analysed on a curved surface whose ambient surroundings are stratified but not necessarily linear. Various gradients in the core will be considered so that the decelerating effects of various external stratifications on the boundary layer will be made clear.

A method similar to that used by [28] is employed. The series forms used were suggested originally by [29], who studied an external boundary layer flow with an unstratified ambient liquid. His analysis will be extended here to include the latter effect. Eqns. (1.8) to (1.10) will be used but due to the effect of variable core temperature (assuming a quasi-steady state), eqn. (1.10) will be rewritten as:

$$u \frac{\partial \theta}{\partial x} + v \frac{\partial \theta}{\partial y} = \frac{\bar{\nu}}{Pr} \frac{\partial^2 \theta}{\partial y^2} - u \frac{dT_\infty}{dx} \qquad (3.18)$$

The solution of eqns. (1.8), (1.9) and (3.18) is outlined in Appendix B where a series expansion method is employed. Three different core stratifications are considered as follows:

$$\begin{aligned} &(1) \quad A = \phi + \phi^2 \\ &(2) \quad A = \phi + \phi^2/2 \\ &(3) \quad A = \phi + \phi^2/4 \\ &(4) \quad A = 0 \end{aligned} \qquad (3.19)$$

where A is the non-dimensional temperature variation in the core liquid.

The effect of external stratification shows itself with the injection of warm liquid into the surrounding medium, thus resulting in the thinning of momentum boundary layer. In Fig. 7 this thinning is shown to become greater as the temperature gradient outside the boundary increases.

The external temperature gradient has a deaccelerating effect on the boundary layer, similar to an adverse pressure gradient in forced flow. Naturally, the driving force in free convection is the temperature difference between the core and the point of interest. Once this difference becomes smaller in the downstream direction, the flow deaccelerates.

In the present analysis, an isothermal core is considered but once the liquid is completely stratified, this approach is not sufficient and one must solve the perturbation equations along with the energy and mass equations (3.1) and (3.5).

3.7 Results and Discussions

Data from experiments with R11 for two different fill heights are plotted along with the analytical predictions in Figs. 8 and 9 with and without the internal protection material EXPLOSAFE. The proposed approach leads to very close agreement despite the simplifying assumptions utilized in its development. The third order profile given in eqn. (3.8) appears to represent the thermal stratification

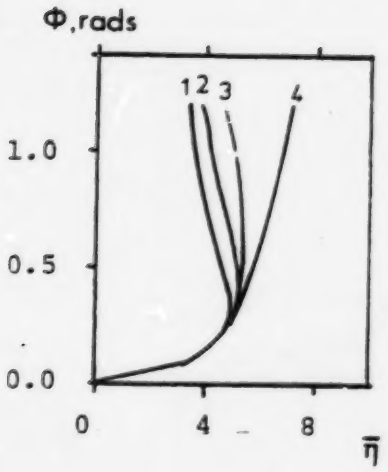

FIGURE 7. Momentum boundary layer for various degrees of external stratification (curves 1,2,3 and 4 are defined in text ,eqns. 3.19) .

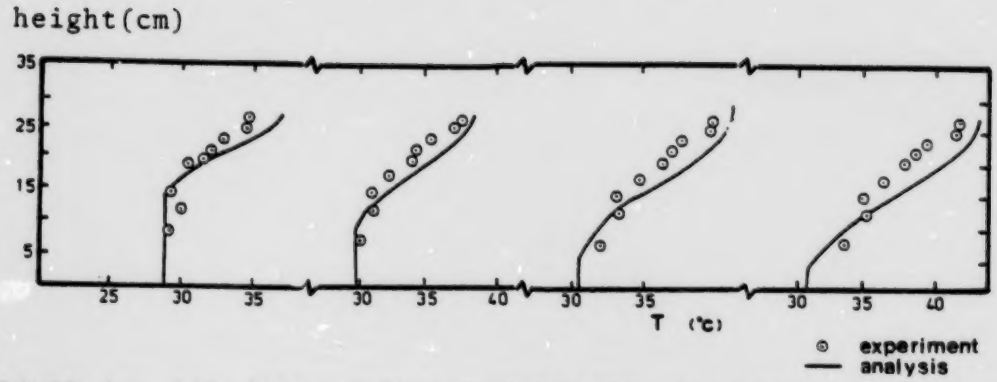

FIGURE 8. 80% fill, with 1" EXPLOSAFE. Transient development of vertical temperature gradient(q=40 kw/sq. m) .

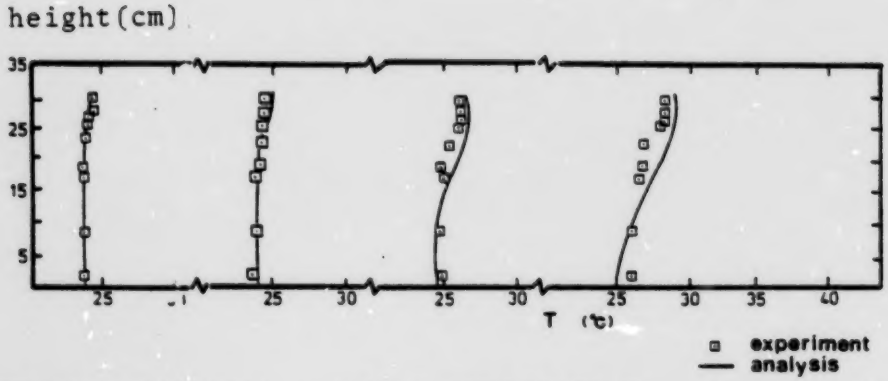

FIGURE 9. 85% fill, without EXPLOSAFE.Transient development of vertical temperature gradient (q=20 kw/sq.m) .

profile adequately for both cases. For filling ratios below 30 percent by volume, a lumped analysis can be made since this angle approximately represents the stability for side wall boundary layer commencement.

In the present analysis, the liquid-vapor interface is assumed adiabatic due to the experimentally observed temperature profiles (see Fig. 3) and the very small amount of condensation taking place resulting from the vapor being compressed due both to heating and from the liquid thermal expansion.

Large discrepancies are observed between the experimental and analytical results for vertical cylinders heated from the side due to the differences in the heat transfer mechanism [16]. This perhaps is due to the mixing of the low velocity eddies generated in these boundary layers with the downward moving core fluid. This process is self sustaining as the core velocities are appreciable and create a reverse shear in the outer boundary region causing further enhancement of the turbulent mixing. If this mixing is neglected, the interface temperatures are over-predicted as in [15] or [16]. Ref. [30] has observed this type of mixing and concluded that it was one of the causes of ambient fluid heating.

Boundary layer heat loss due to external stratification and due to eddy mixing are quite distinct. The first is

a result of decreasing buoyancy forces while the latter mechanism is caused by the reverse shear between the core and boundary layer.

In the partially filled horizontal cylinder large downward velocities are absent due to the mixing of the core fluid with the fluid issuing from the unstable region located on the concave bottom of the cylinder. In this region the heated fluid moves directly vertically upwards to mix with the downward moving fluid from the stratified layer, reducing the effect of reverse shear and enhancing the mixing to provide a near isothermal but time dependent core temperature.

This latter effect is accounted for in the presented analysis by the instability analysis since this provides the primary energy content to the core. In the previous sections a simple force balance was utilized to provide criteria for the end of this unstable region so to mark the formation of the stable boundary layer. Once this layer is formed, the usual equations of motion, eqns. (2.1) and (2.2) govern the flow since the centrifugal force acts in a direction perpendicular to the flow.

CHAPTER IV

A FINITE DIFFERENCE SOLUTION

4.1 Introduction

In this chapter, a numerical approach will be applied to the present problem where equations (1.1) to (1.2) along with the continuity equation (1.3) are integrated using finite differences. The above mentioned equations can be rewritten in cartesian coordinates (since $g_x = 0$ in this system) and transformed to vorticity-stream function equations through the elimination of the pressure gradient term resulting in [7]

Vorticity:

$$\frac{\partial W}{\partial \tau^+} + U\frac{\partial W}{\partial X} + V\frac{\partial W}{\partial Y} = \frac{\partial \theta}{\partial X} + \frac{1}{\sqrt{Gr_R}}\nabla^2 W \qquad (4.1.a)$$

Energy:

$$\frac{\partial \theta}{\partial \tau^+} + U\frac{\partial \theta}{\partial X} + V\frac{\partial \theta}{\partial Y} = \frac{1}{Pr\sqrt{Gr_R}}\nabla^2 \theta \qquad (4.1.b)$$

Stream Function:

$$\nabla^2 \psi = -W \qquad (4.1.c)$$

Velocity Relations:

$$U = \frac{\partial \psi}{\partial Y}, \quad V = -\frac{\partial \psi}{\partial X} \qquad (4.1.d)$$

where

$$U = u/u_\infty,\ V = v/u_\infty,\ X = x_c/R,\ Y = y_c/R,$$

$$\theta = (T-T_\infty)\frac{k}{qR} \quad \text{if} \quad Gr_R = \frac{g\beta qR^4}{k\nu^2} \quad (\text{where } U_\infty = \sqrt{\frac{g\beta qR^2}{k}})$$

$$\text{or } \theta = \frac{T-T_\infty}{T_\omega-T_\infty} \quad \text{if} \quad Gr_R = \frac{g\beta\Delta TR^3}{\nu^2} \quad (\text{where } U_\infty = \sqrt{g\beta\Delta TR})$$

$$\tau^+ = \frac{\nu}{R^2}\sqrt{Gr_R}\ t$$

The above equations have been solved by many researchers with various boundary conditions. In general their applicability is limited to two dimensions since it is not possible to find a scalar potential to satisfy the continuity equation in three dimensions. However [32] outlines a technique originally introduced by [33] called vector potential method which can be used to solve such flows. In the present study a two-dimensional flow is assumed.

A numerical approach is necessary if one needs to have a qualitative as well as more detailed quantitative information. The integral technique presented earlier cannot meet this requirement although it can give good predictions in an averaged sense.

4.2 The Difficulties Associated With the Geometry and A Possible Approach

Although eqs. (4.1) are solvable with a suitable finite

difference method, there are difficulties associated with the geometry of the solution domain (see Fig. 1). Due to the partial filling the coordinate system used does not coincide with the boundaries of the region, hence there will be some trouble in locating the control volume boundaries at the interface. The polar coordinate system as well as any others commonly used will fail to give regular mesh points in this region. One is therefore forced to choose the coordinate system such that it will exactly fit the boundaries of the solution domain. Such a method is not completely new, however, it is problem dependent. That is, one has to use special transforms for different problems. An example in such an application is [34], where natural convection along a vertical wavy surface was considered and transformed to a flat surface by a very special relation.

The transformation introduced in this study is also special but it can further be applied to other geometries provided certain requirements are met. This is discussed below.

The method is indeed a stretching of the X-coordinate(*) by normalizing it using the cord length associated with the Y-coordinate of an arbitrary point. In this way, an

---

(*)Note that we are dealing with Cartesian coordinates instead of polar since expressed in the latter, the transformed equations are extremely complicated.

orthogonal system can be obtained in (ζ,η) where

$$\zeta = \frac{X}{\sqrt{1-Y^2}} \quad \text{and} \quad \eta = Y \tag{4.2}$$

Note that $-1 \leq \zeta \leq 1$ and $-1 < Y < 1$ assuming the circle is centered originally at (0,0).

The result of this transformation can be seen in Figure 10, where the original circle is mapped onto a square or the partially filled region to a rectangle. It can be seen that

$$L(Y) = \sqrt{1-Y^2} \times 2$$

is the associated cord length which varies with height.

The above technique can be applied to any domain whose solid walls can be expressed with a continuous function which also possesses continuous first derivatives in the domain of interest.

To consider a few examples consider a parabolic container given by ($Y \geq 0$ for all X),

$$Y = a X^2$$

where a is a constant ($a > 0$) we can write

$$\zeta = \frac{X}{\sqrt{Y/a}}, \quad \eta = Y \tag{4.3}$$

or for an elliptic container given by

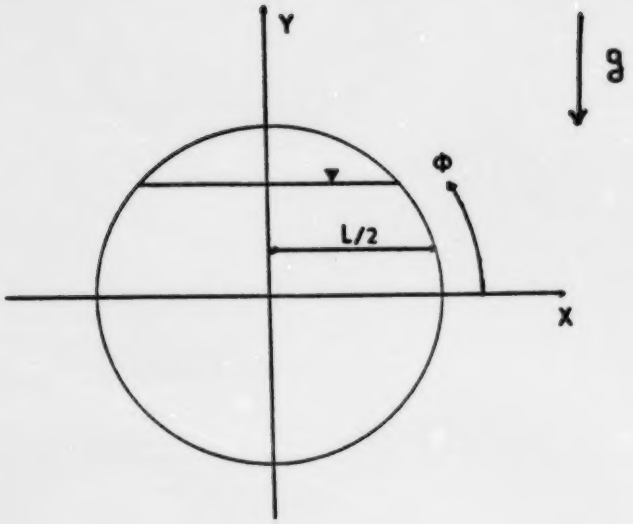

FIGURE 10.a Physical plane.

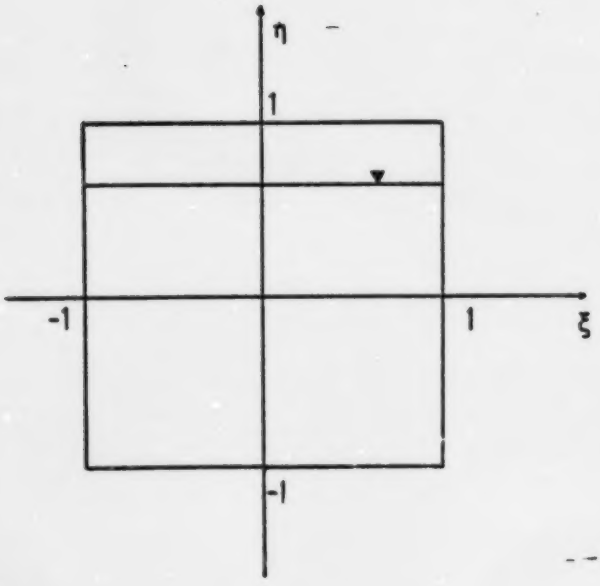

FIGURE 10.b Mathematical plane.

$$\frac{X^2}{a^2} + \frac{Y^2}{b^2} = 1,$$

(4.4)

$$\zeta = \frac{X}{\sqrt{a^2 - \left(\frac{aY}{b}\right)^2}}, \quad \eta = Y$$

Similar expressions can be written for any curve meeting the above continuity requirements. Note that if these containers are full, it is much easier to use the conventional coordinates (say elliptic coordinates), however if they are partially full, then the above transformations simplify the problem a great deal.

The drawback of this method is the additional complication of eqn. (4.1). These have to be transformed according to the relations given by eqn. (4.2). The relevant operators appearing in eqn. (4.1) can be written as:

$$\nabla^2_{X,Y} = \nabla^2\zeta \frac{\partial}{\partial\zeta} + \nabla^2\eta \frac{\partial}{\partial\eta} + \nabla\zeta\cdot\nabla\zeta \frac{\partial}{\partial\zeta} + \overline{\nabla}\eta\cdot\overline{\nabla}\eta \frac{\partial^2}{\partial\eta^2} + 2\overline{\nabla}\zeta\cdot\overline{\nabla}\eta \frac{\partial^2}{\partial\zeta\partial\eta}$$

$$\frac{\partial}{\partial X} = \frac{\partial\zeta}{\partial X}\frac{\partial}{\partial\zeta} + \frac{\partial\eta}{\partial X}\frac{\partial}{\partial\eta} \qquad (4.5)$$

$$\frac{\partial}{\partial Y} = \frac{\partial\zeta}{\partial Y}\frac{\partial}{\partial\zeta} + \frac{\partial\eta}{\partial Y}\frac{\partial}{\partial\eta}$$

which, using eqn. (4.2), reduces to

$$\nabla^2_{X,y} = \zeta \frac{(1+2\eta^2)}{(1-\eta^2)^2} \frac{\partial}{\partial \zeta} + \left[\frac{1}{1-\eta^2} + \left(\frac{\zeta\eta}{1-\eta^2}\right)^2\right] \frac{\partial^2}{\partial \zeta^2} + \frac{\partial^2}{\partial \eta^2} + \frac{2\zeta\eta}{1-\eta^2} \frac{\partial^2}{\partial \zeta \partial \eta}$$

$$\frac{\partial}{\partial X} = \frac{1}{\sqrt{1-\eta^2}} \frac{\partial}{\partial X} \tag{4.6}$$

$$\frac{\partial}{\partial Y} = \frac{\zeta\eta}{1-\eta^2} \frac{\partial}{\partial \zeta} + \frac{\partial}{\partial \eta}$$

Equations (4.1) are given in Appendix C in the rewritten form as they appear in the mathematical plane of Figure (10.b).

It is important to check the "one-to-oneness" of equation (4.2),

$$\overline{\nabla}_{X,Y} = \begin{Bmatrix} \frac{\partial}{\partial X} \\ \frac{\partial}{\partial Y} \end{Bmatrix} = \underbrace{\begin{bmatrix} \frac{\partial \zeta}{\partial X} & \frac{\partial \eta}{\partial X} \\ \frac{\partial \zeta}{\partial Y} & \frac{\partial \eta}{\partial Y} \end{bmatrix}}_{M} \begin{Bmatrix} \frac{\partial}{\partial \zeta} \\ \frac{\partial}{\partial \eta} \end{Bmatrix} \tag{4.7}$$

For a one-to-one inversion the above system has to be invertible (for a unique inversion $|M| \neq 0$) which reduces to the condition

$$|M| = 1-Y^2 \neq 0 \quad \text{or} \quad Y \neq \mp 1 \tag{4.8}$$

This is to be expected since the vertical lines in the ζ,η plane meet at a single point in the X,Y plane as these lines approach $\eta = \mp 1$, resulting in a singular transformation.

The singularity at $\eta = 1$ is however avoided naturally since the problem is a partially filled one. The singularity at the bottom, i.e. $\eta = -1$ is excluded from the domain by utilizing an infinitesmal horizontal cut of approximately 1% of the radius; that is a cut at $\eta = -0.99$ or 0.5% of the total width. The computations for the completely filled cylinders were also treated in the same way, taking a cut at $\eta = 0.99$. As will be demonstrated, these approximations do not significantly affect the results.

4.3 The Boundary Conditions

The boundary conditions must be treated in a different form than the usual manner. Note first that there are no vorticity equations now but only a set of partial differential equations to be solved.

Not much of a problem arises with Dirichlet type boundary conditions for instance, a constant prescribed temperature can be realized by imposing the same value along the walls of the rectangular domain. The same applies to the stream function.

The wall values of the vorticity are computed from the stream function values in the usual way but the treatment is different due to the cross derivative term appearing in the Laplacian of eqn. (4.1.c) (or eqn. (C.3) in Appendix C).

Noting(*) along the walls of the rectangle,

$$V = \frac{1}{\sqrt{1-\eta^2}} \frac{\partial \psi}{\partial \zeta} = 0 \quad \text{and} \quad U = \frac{\partial \psi}{\partial \eta} \cdot \frac{\partial^2 \psi}{\partial \eta^2} = 0 \qquad (4.9)$$

we can write eqn. (B.3) using eqn. (4.9) as:

$$\frac{1}{1-\eta^2} + \left(\frac{\zeta\eta}{1-\eta^2}\right)^2 \frac{\partial^2 \psi}{\partial \zeta^2} + \frac{2\zeta\eta}{1-\eta^2} \frac{\partial^2 \psi}{\partial \zeta \partial \eta} = -W \qquad (4.10)$$

Now $\frac{\partial^2 \psi}{\partial \zeta^2}$ can be approximated to third order accuracy using eqn. (4.9) and a Taylor series expansion (see Figure 11),

$$\frac{\partial^2 \psi}{\partial \zeta^2} = \frac{\gamma \psi_{i+1,j} - \psi_{i+2,j}}{2\Delta\zeta^2} \qquad (4.11)$$

similarly,

$$\frac{\partial^2 \psi}{\partial \zeta \partial \eta} = \frac{-\partial}{\partial \zeta} \left(\frac{\partial \psi}{\partial \eta}\right).$$

Expanding in Taylor series again, having i located at the left wall, (i.e. i = 1),

$$\left.\frac{\partial \psi}{\partial \eta}\right|_{i+1} = \cancel{\left.\frac{\partial \psi}{\partial \eta}\right|_i}^{0} + \frac{\partial}{\partial \zeta} \left(\frac{\partial \psi}{\partial \eta}\right)\Big|_i \Delta\zeta + \frac{\partial^2}{\partial \zeta^2} \left(\frac{\partial \psi}{\partial \eta}\right)\Big|_i \frac{\Delta\zeta^2}{2!} + O(\Delta\zeta^3) \qquad (4.12.a)$$

$$\left.\frac{\partial \psi}{\partial \eta}\right|_{i+2} = \cancel{\left.\frac{\partial \psi}{\partial \eta}\right|_i}^{0} + \frac{\partial}{\partial \zeta} \left(\frac{\partial \psi}{\partial \eta}\right)\Big|_i 2\Delta\zeta + \frac{\partial^2}{\partial \zeta^2} \left(\frac{\partial \psi}{\partial \eta}\right)\Big|_i \frac{(2\Delta\zeta)^2}{2!} + O(\Delta\zeta^3) \qquad (4.12.b)$$

(*) Note that this follows from eqn. (4.5) since $\frac{\partial \psi}{\partial \zeta} = 0$ due to V = 0 at the wall.

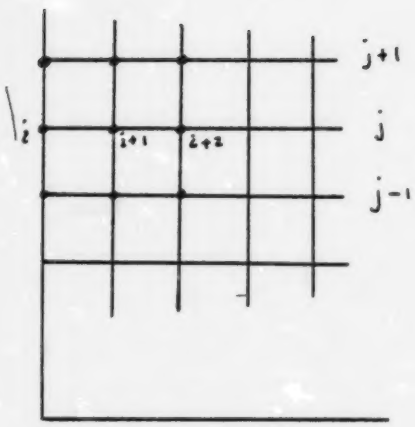

FIGURE 11. Grid system for wall vorticity (at left i=1) .

Eliminating $\frac{\partial^2}{\partial\zeta^2}\left(\frac{\partial\psi}{\partial\eta}\right)\Big|_i$ in above, we obtain,

$$\frac{\partial}{\partial\zeta}\left(\frac{\partial\psi}{\partial\eta}\right)_i = \frac{4\left.\frac{\partial\psi}{\partial\eta}\right|_{i+1} - \left.\frac{\partial\psi}{\partial\eta}\right|_{i+2}}{2\Delta\zeta} \qquad (4.13)$$

with second order accuracy. A similar expression can be written for the right wall with i+1 → k-1, i+2 → k-2 and i → k where k is the total number of nodes in ζ direction.

Note that at the bottom and top of the fully filled cylinder we have,

$$\frac{\partial^2\psi}{\partial\eta^2} + \frac{2\zeta\eta}{1-\eta^2}\frac{\partial^2\psi}{\partial\zeta\partial\eta} = -W \qquad (4.14)$$

since derivatives $\frac{\partial}{\partial\zeta}$ vanish at the horizontal boundaries (ψ = const.). At the shear free surface eqn. (4.14) simplifies to W = 0. The discretization of eqn. (4.13) which with central differences requires 9 nodal points at every station along the wall, whereas in a real rectangular enclosure one has to consider only three nodes. This is a drawback of the present method.

For the energy equation (B.2), the Dirichlet type boundary conditions do not introduce any difficulty as stated before. However Neumann boundary conditions must be treated carefully as follows: if the heat flux is specified in non-dimensional form we can write:

$$\frac{\partial\theta}{\partial X} = \cos\Phi \text{ and } \frac{\partial\theta}{\partial Y} = \sin\Phi \qquad (4.15)$$

The assumption of normal heat flux vector on the wall is a reasonable one. That is, $\Phi = \phi$ and this leads to

$$\cos\phi = X = \zeta\sqrt{1-\eta^2} \quad \text{and} \quad \sin\phi = Y = \eta \tag{4.16}$$

Therefore eqn. (4.15) is rewritten according to eqns. (4.5) and (4.15) as:

$$\frac{1}{\sqrt{1-\eta^2}} \frac{\partial\theta}{\partial\zeta} = \zeta\sqrt{1-\eta^2} \rightarrow \frac{\partial\theta}{\partial\zeta} = \zeta(1-\eta^2) \tag{4.17.a}$$

and

$$\frac{\zeta\eta}{1-\eta^2} \frac{\partial\theta}{\partial\zeta} + \frac{\partial\theta}{\partial\eta} = \eta \tag{4.17.b}$$

Substituting eqn. (4.17.a) in (4.17.b) results in

$$\frac{\partial\theta}{\partial\eta} = \eta(1-\zeta^2) \tag{4.18}$$

which is zero at either the left or right walls since $\zeta^2 = 1$. As will be seen later, the isotherms indicate fairly uniform temperatures close to the wall in the flow direction until a region close to the interface, where sharp changes in the temperature field are expected. Thus, it is obvious that eqn. (4.18) is satisfied indirectly by imposing eqn. (4.17.a) as a boundary condition. Finer grids of course will result in better apoximations near the interface.(*)

The stream function ψ is zero on all the boundaries

(*)Note that it is relatively easy to choose a non-uniform contracting mesh system close to the interface in the ζ-η plane without paying attention to their actual shapes in the physical domain.

since there is no net mass transfer either across the wall or the interface.

4.4 Discretization in the ζ-η Plane, Disadvantages and Advantages

Eqns. (C.1) to (C.4) in Appendix C are discretized using central differences with an implicit representation in time (Appendix D). In other words, second order accuracy in space derivatives and first order accuracy in time derivatives are utilized. The scheme is unconditionally stable for all $\Delta\tau^+$. It was observed however that a very heavy underrelaxation should be used in eqn. (C.3). This was as low as 0.001 for $Gr = 1 \times 10^7$, $Pr = 0.72$ while the highest allowable value was 0.5 for $Gr = 114$, $Pr = 6380$. It should be noted that throughout the computation the vorticity transport equation was not underrelaxed assuming a relaxation coefficient of unity. The flow seemed to be very sensitive to changes in the stream function field and the development of the flow had to be decelerated. This may be due to the direct effect of stream function on the velocity components U and V (see eqn. 4.1.d).

Despite this, the advantages brought by the transformation are obvious:

1) It is possible to choose a rectangular grid throughout the domain without any difficulty at the interface.

2) One can use central differences with conventional orders of accuracy. That is, since the coordinate system is orthogonal, the Taylor series expansions are valid in their original form but in ζ and η.
3) One has the freedom to choose $\Delta\zeta = \Delta\eta$ so that the truncation error introduced by the Taylor series expansion is minimized.

4.5 Solution Method and Algorithm

The discretized equations given in Appendix D are solved both with a line by line (a combination of Gauss-Seidel and TDMA methods) and the Gauss-Seidel point by point method. The traversing direction in the former was chosen to be from bottom to top with horizontal lines (i.e. TDM was written in a horizontal direction).

In the point by point Gauss-Seidel method left to right sweeps from bottom to top are made. No significant improvement was noted with respect to the computation time between the two methods.

The computation algorithm can be summarized as follows:

a) initialize all the field variables and impose any Dirichlet type boundary conditions if any;
b) compute the vorticity field from eqn. (D.1);
c) compute the temperature field from eqn. (D.2);
d) compute the stream function field from (D.3);

e) correct the vorticity boundary conditions at the wall using eqn. (4.13) (or its analog at the right wall) and the discretized form of eqn. (4.14), at the bottom and top. For a shear free interface set $W = 0$;

f) check convergence to within 0.001% of the maximum relative change in the vorticity field. That is,

$$\max\left|\frac{W_{i,j}^{n+1} - W_{i,j}^{n}}{W_{i,j}^{n+1}}\right| \times 100 \leq 0.001$$

where n refers to the time level.

Here, it is assumed that convergence is achieved when the vorticity field meets the above requirement;

g) start from (b) if no convergence or if convergence is achieved, then: store the computed fields and increase time, starting at (b), use the old values as initial guesses for the new field variables; and

h) if the transient is over, then do the inverse mapping of the coordinates and interpolate for the constant field variables for stream function (or temperature or heat lines) and draw contours for it. Print the computation results.

A flow diagram for the computer programme is given in Appendix E.

4.6 Test Runs

Published experimental data for completely filled cylinders are available with Prandtl numbers 19950 and 0.7 (silicone oil and air, respectively). Data are given for a case where the walls of the cylinder were kept at constant temperature with a saw-tooth distribution in [6]. The computed steady state velocity and temperature profiles are plotted against the experimental values in Fig. 12 and Fig. 13. The comparison is good considering the assumptions made in the model equations. The mathematical plane was chosen to be $-1 \leq \zeta \leq 1$ with $-0.99 \leq \eta \leq 0.99$ to exclude the singularities. Initially, with two eddies formed the flow developed in either half of the cylinder. These grow larger with time as the streamlines merge into each other and form a single elliptical cell. As steady state is approached, however two small cells remain, rotating in a counter-clockwise direction. These eddies are shown in an enlarged velocity vector diagram in Fig. 14. Ref. [2] was however, unable to resolve these in his steady state solutions for this case, where a modified Oseen linearization was used. In the present computation, these cells were too small to be detected with a grid size of $\Delta\zeta = 0.1$ (20×20 mesh), hence a 40×40 mesh configuration was chosen to determine their existence.

The results of the temperature and velocity profiles with $Pr = 0.7$, $Gr = 4.5\ \ 10^4$ are shown in Fig. 15 and Fig. 16.

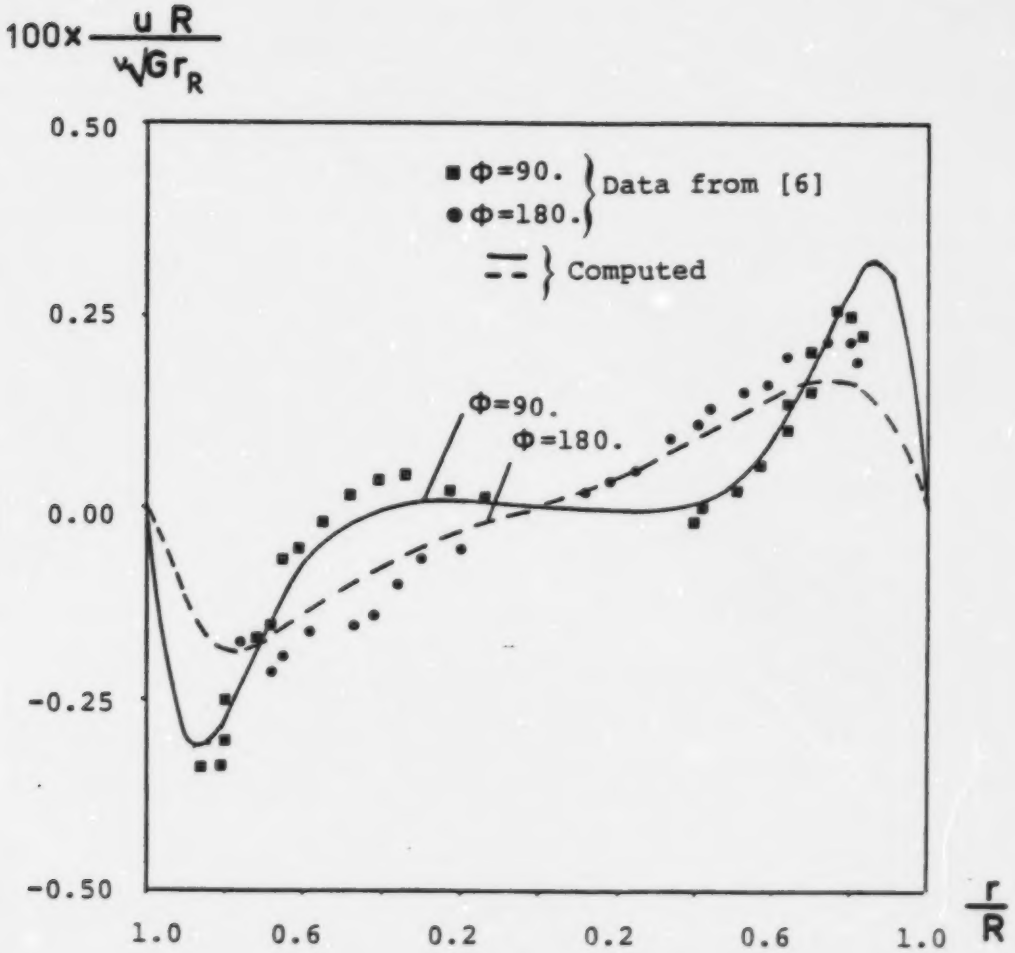

FIGURE 12. v elocity profiles for Pr=19950., Gr=1.1 .

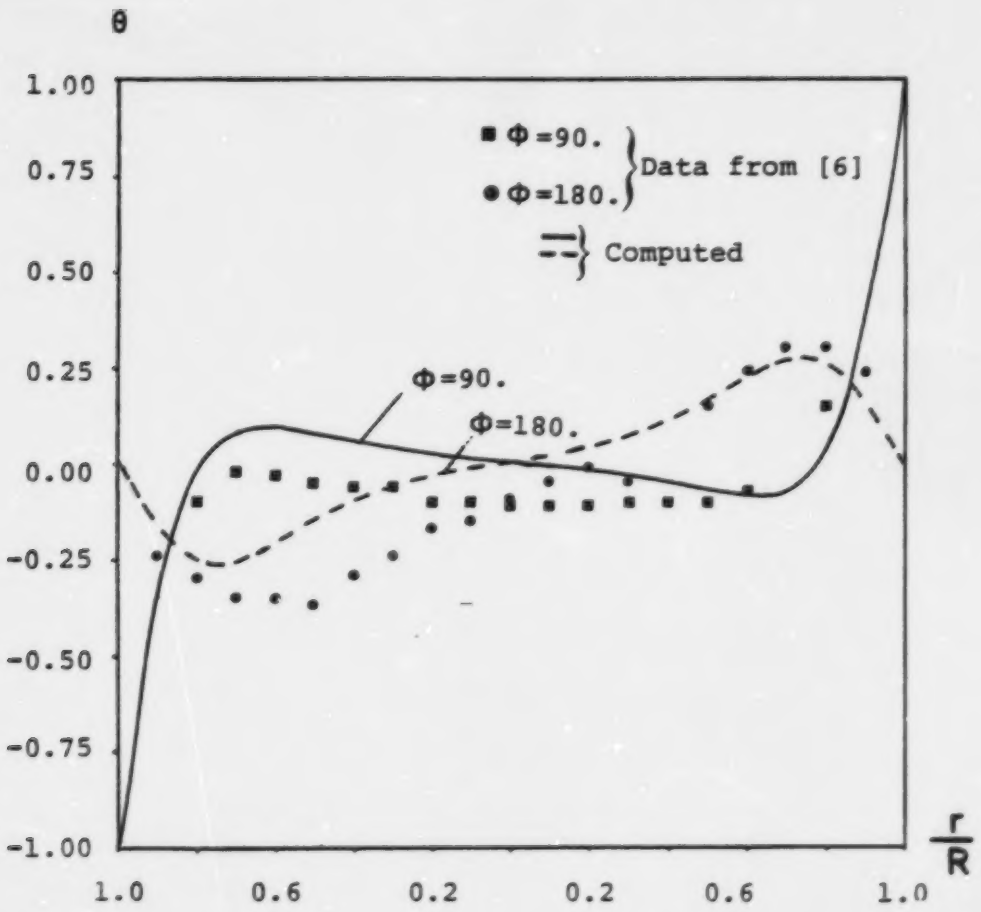

FIGURE 13. Temperature profiles for Pr=19950., Gr=1.1 .

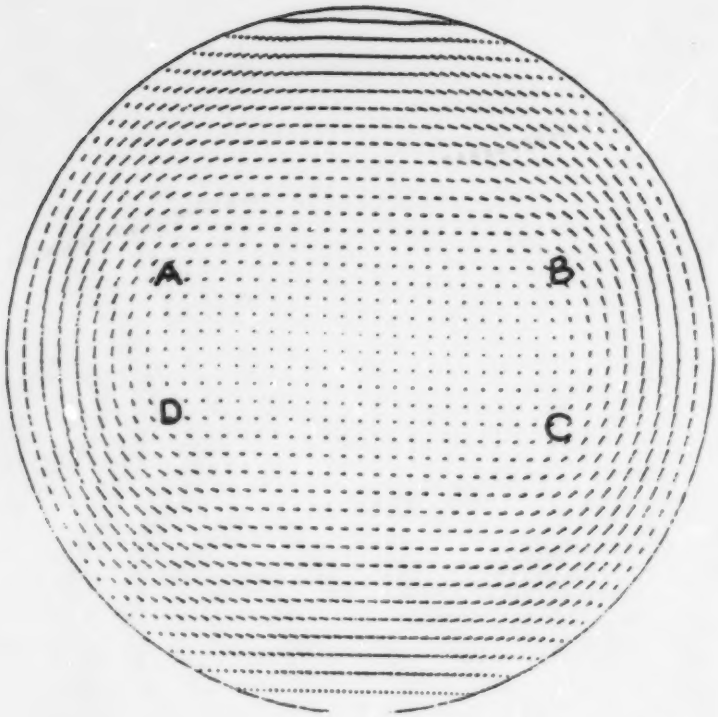

FIGURE 14.a Velocity vector plot after steady state computations for Pr=19950.,Gr=1.1, 40x40 mesh.

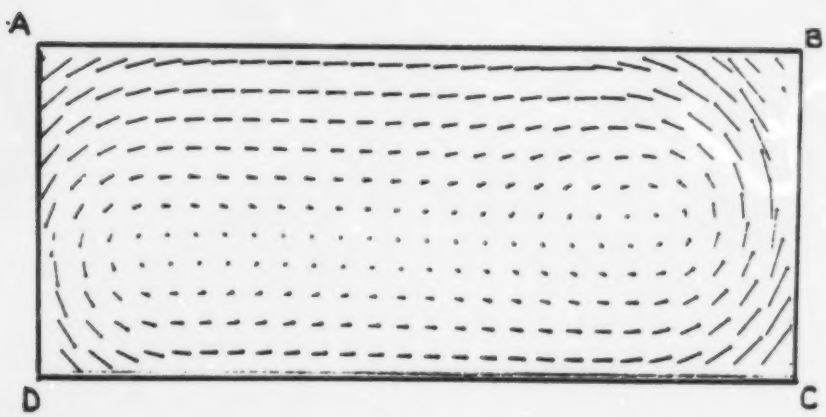

FIGURE 14.b Enlarged central core with two rotating eddies.

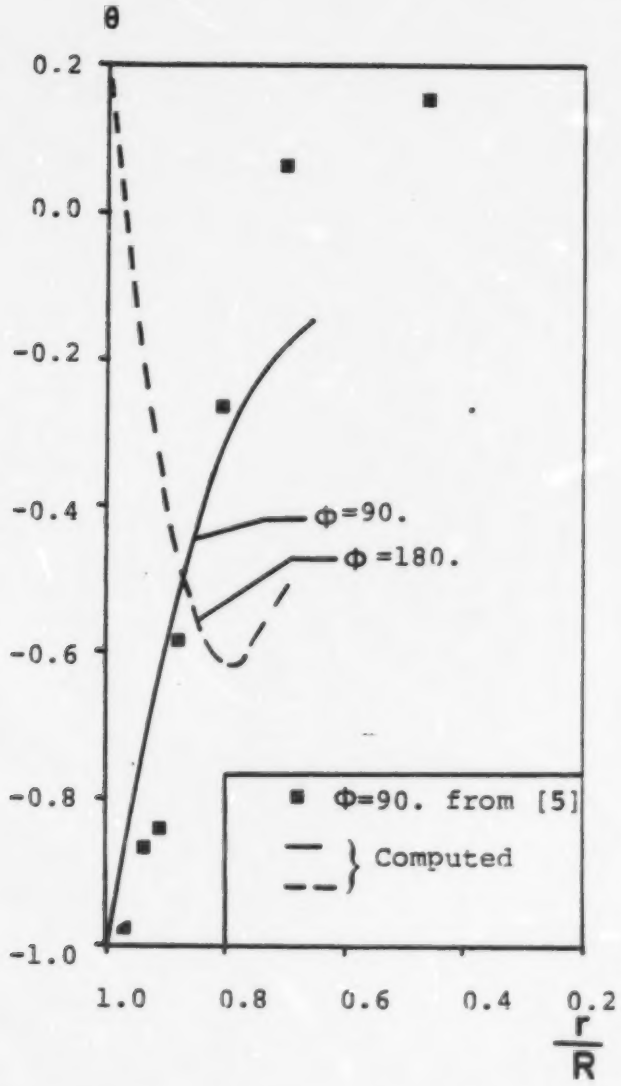

FIGURE 15. Temperature profiles for Pr=0.7, $Gr=4.5x10^{5}$.

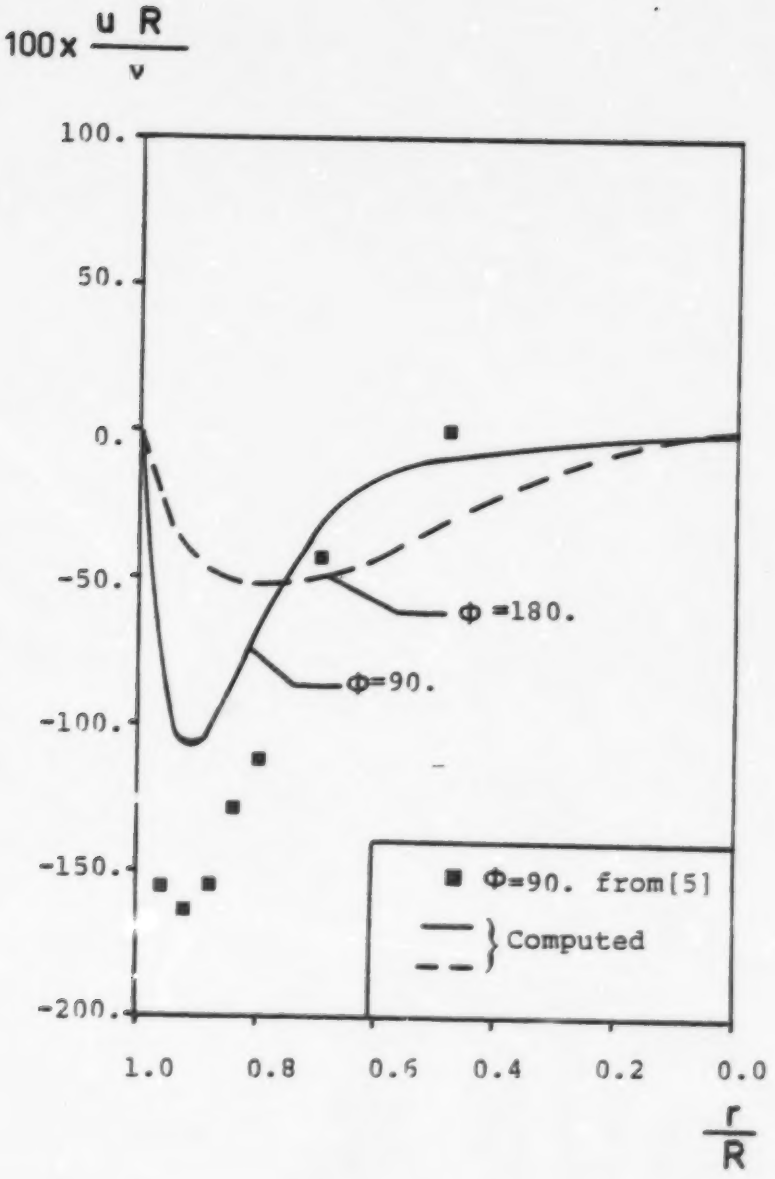

FIGURE 16. Velocity profiles for Pr=0.7, Gr=4.5x10^4 .

where they are compared with the data of [5]. In this case, the cylinder halves were kept at two different temperatures. The agreement with the steady state velocity profiles is not as good as the temperature profile. No indication of rotating cells were found for this test run even with a 40×40 mesh. This may be due to the rapid diffusion of heat from the walls of the cylinder to the interior regions, resulting in less steep temperature gradients as can also be observed in Fig. 17.a and Fig. 17.b.

For the case of the partially filled vessel, which is the main objective of this study, glycerine, a high Prandtl number liquid was chosen for the simulation runs. It should be noted that now the solution domain is $-1 \leq \zeta \leq 1$, $-0.99 \leq \eta \leq 0.4$ where $\eta = 0.4$ corresponds to a 75% filling.

The flow conditions are such that $Gr_R^* = 114$ and $Pr = 6380$. Since the properties are assumed constant along with the heat flux, these values do not change during the computation.

The simulated flow starts with two small eddies at the tank walls close to $\phi = 90°$ (Fig. 18.a). Eventually the two rotating cells join at the centre (Fig. 18.b) and a distortion is observed along the line of their contact (Fig. 18.c).

The shape of the innermost eddies before and after the contact can be explained as follows: consider only one-half of the cylinder, say the left, the developing cell in

FIGURE 17.a Steady state isothermals for Pr=19950., Gr=1.1 .

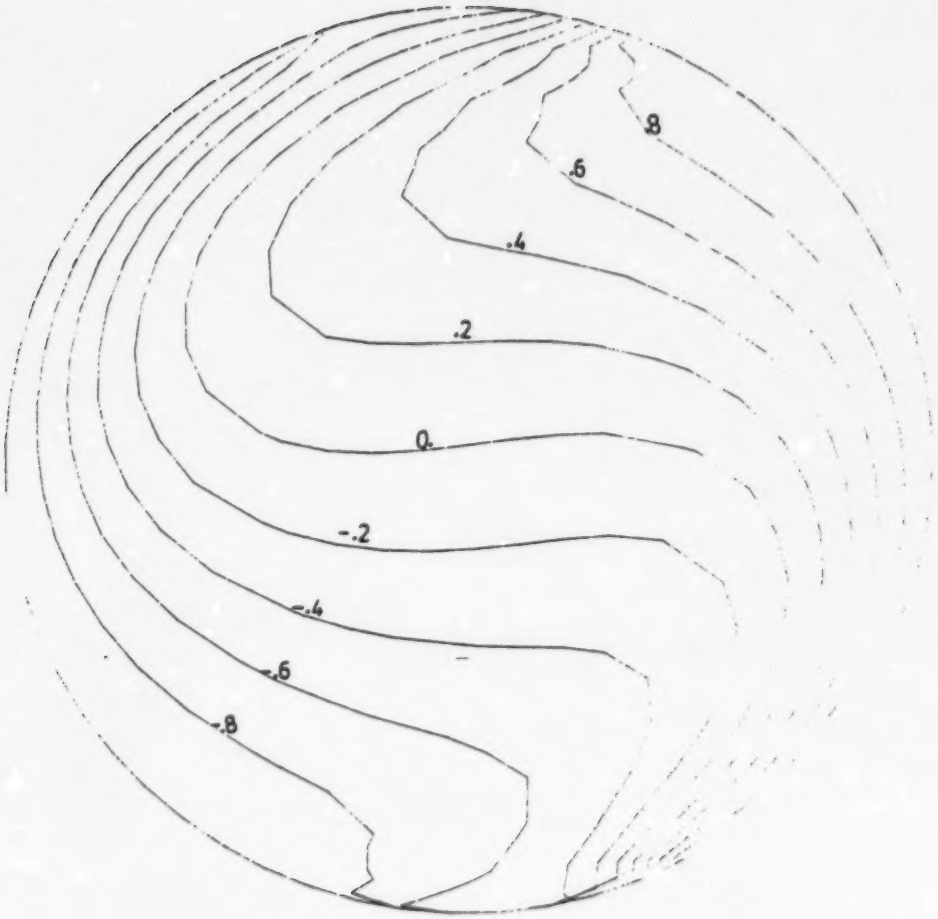

FIGURE 17.b Steady state isothermals for Pr=0.7, $Gr=4.5x10^4$.

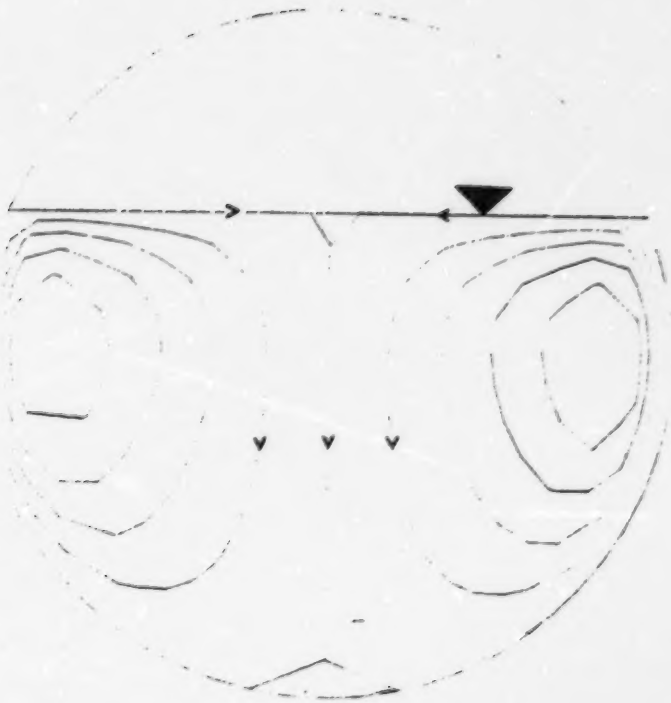

FIGURE 18.a Stream lines in transient computation,Pr=6380., Gr=114., t=0.7 mins.

FIGURE 18.b Stream lines in transient computation,Pr=6380., Gr=114., t=3.3 mins.

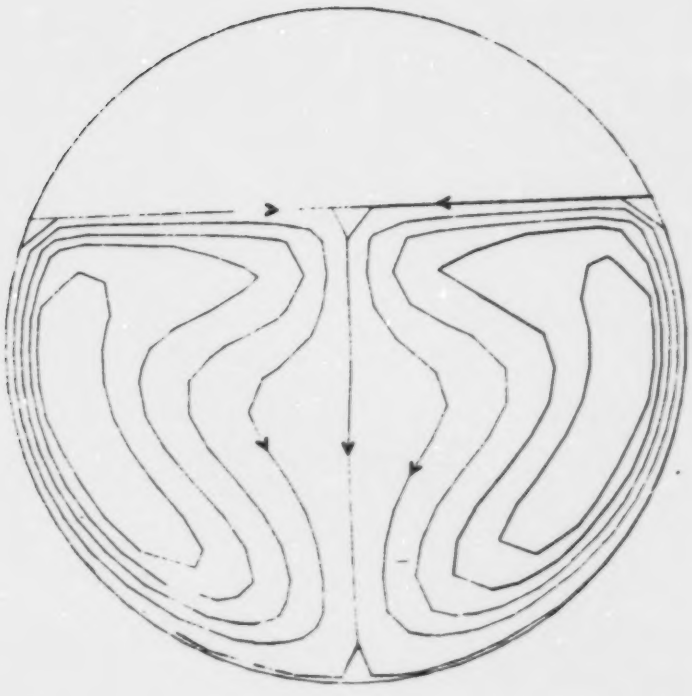

FIGURE 18.c Stream lines in transient computation,Pr=6380., Gr=114., t=4.6 mins.

this region would continue to grow indefinitely with the flow velocities increasing if there were no other cell in the other half of the cylinder. However when they meet at the centre since the other is rotating in the opposite direction, they cannot grow further, hence the flow must adjust itself to the new situation. Being more explicit, we can say that the inward expansion of the streamlines at the centre is merely due to the increase in effective downward flow area so that the cell, being restricted in its growth, will compensate for this by expanding inwards. Note that the heat flux is always constant and so the flow has to accelerate somehow. Once the above is considered, it is easy to deduce that the flow cannot take any other shape.

The isotherms shown in Fig. 19 for the corresponding times obviously indicate the thermal stratification of the liquid and also the isothermal nature of the core temperatures in a horizontal direction. This was a presumed condition in the previously outlined integral analysis.

Fig. 20 describes the phenomena observed in Fig. 18.c that is, the readjustment of the flow configuration. It can be observed that initially the downward velocity at the interface starts from a zero value, accelerates, and then deaccelerates. When the two eddies join we observe the readjustment where the streamlines distort inwards at $t = 4.6$ mins.

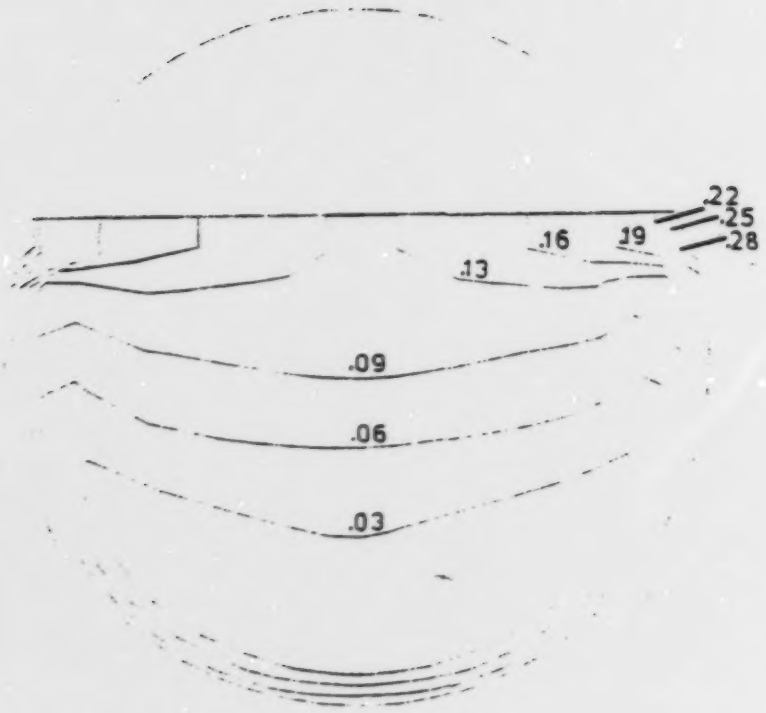

FIGURE 19.a Isothermals in transient computation, Pr=6380., Gr=114., t=0.7 mins.

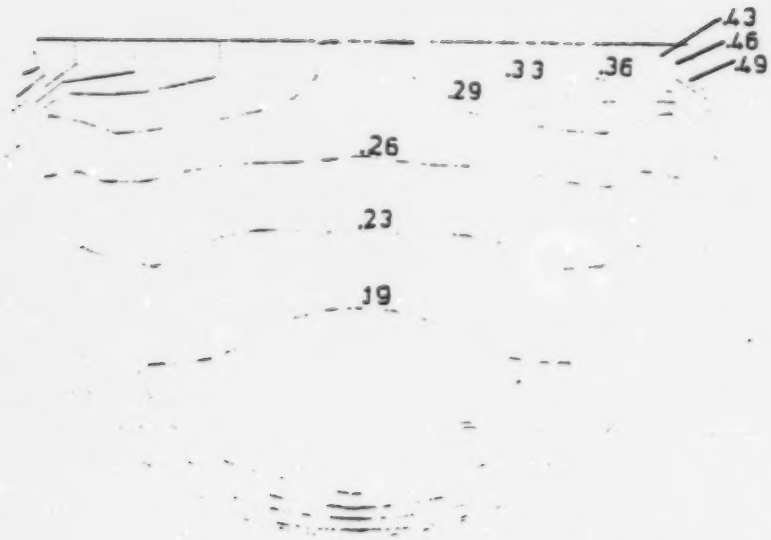

FIGURE 19.b Isothermals in transient computation, Pr=6380., Gr=114., t=3.3 mins.

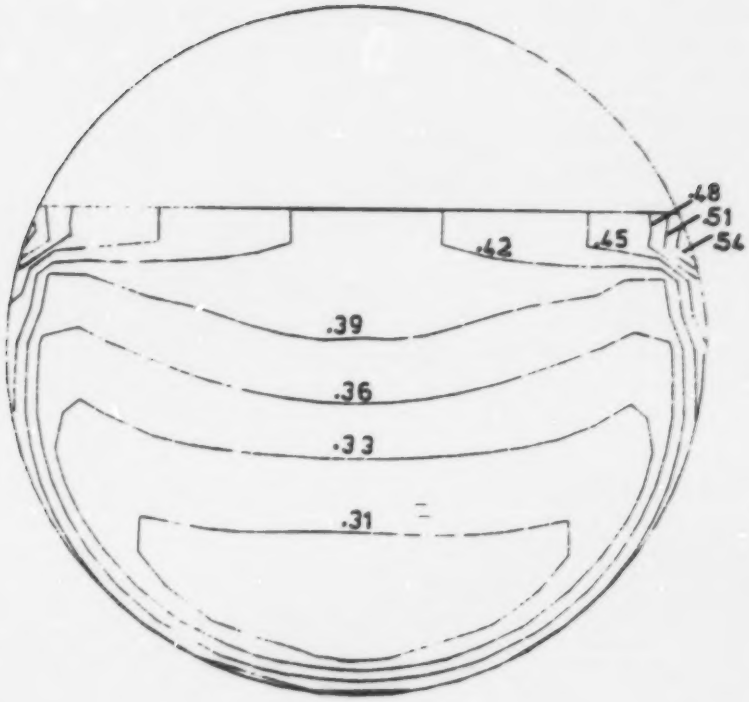

FIGURE 19.c Isothermals in transient computation, Pr=6380., Gr=114., t=4.6 mins.

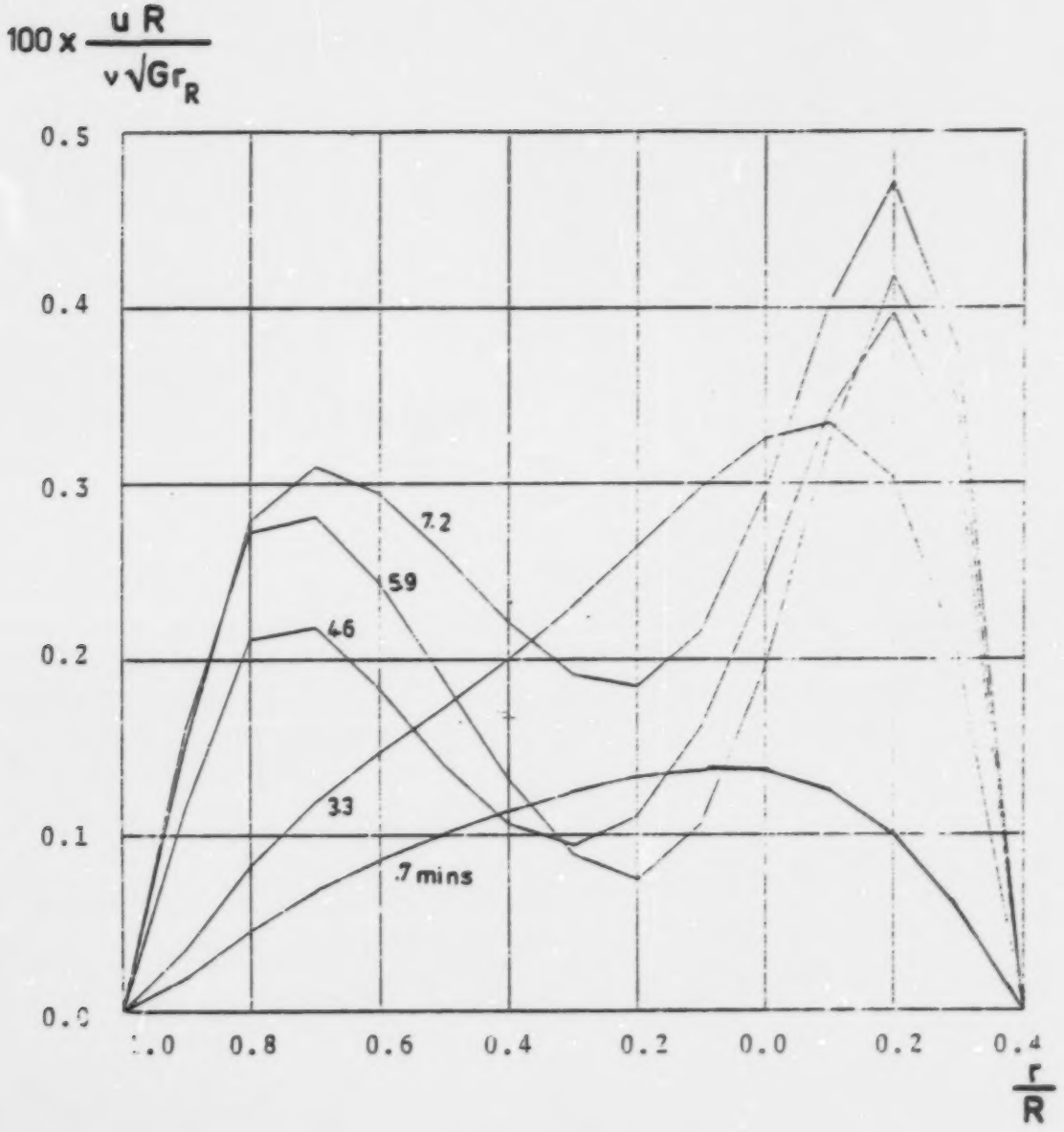

FIGURE 20. Transient central velocities for Pr=6380., Gr=114. (ϕ=180.) .

A flow visualization has qualitatively verified the above results (Fig. 21). Here a tracer was injected into a glass vessel of aspect ratio (length to diameter) of 2, allowed to diffuse and mix uniformly with the glycerine inside. The vessel was filled to about 60% compared to the 75% in the above simulation. Runs for 62% also displayed the same characteristics as in Fig. 18, that is, the streamline distortion occurred close to the centre between the interface and the bottom. The photograph shows a similar development of the streamlines which appear to buckle inwards. This photograph was taken approximately twenty hours after test initiation since it takes a long time for the dye to mix with the liquid completely.

Further information about the flow can be obtained through the visualization of heat flow lines, introduced by [35]. This will be discussed next.

4.7 Heat Lines

The technique of computational heat flow visualization is analogous to the streamline visualization where contours of constant stream values are drawn. The difference is that the stream function satisfies the continuity equation while the "heat function" satisfies the energy equation. Ref. [35] does not give an extension to three dimensional cases, however it is possible that a heat function can also be defined in three dimensions using a vector potential

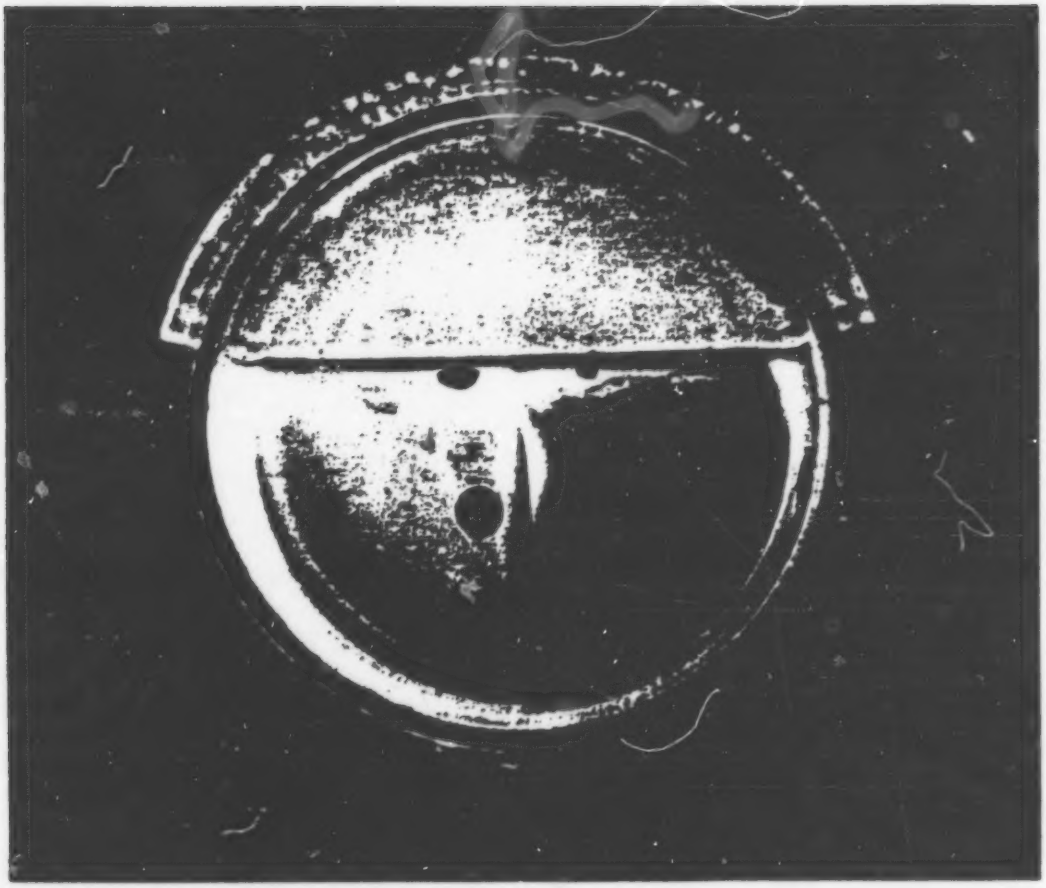

FIGURE 21. Experimental flow pattern for 60% full tank, Pr=6380., Gr=35.

similar to that concept introduced by [33] and discussed in [32].

Consider the energy equation in a quasi-steady state form:

$$u\frac{\partial T}{\partial x_c} + v\frac{\partial T}{\partial y_c} = \alpha\left(\frac{\partial^2 T}{\partial x_c^2} + \frac{\partial^2 T}{\partial y_c^2}\right) \tag{4.18}$$

Using continuity, this can be rewritten as

$$\frac{\partial}{\partial x_c}\left(uT - \alpha\frac{\partial T}{\partial x_c}\right) + \frac{\partial}{\partial y_c}\left(vT - \alpha\frac{\partial T}{\partial y_c}\right) = 0 \tag{4.19}$$

Choosing the heat function such that

$$\frac{\partial H}{\partial y_c} = uT - \alpha\frac{\partial T}{\partial x_c}, \quad -\frac{\partial H}{\partial x_c} = vT - \alpha\frac{\partial T}{\partial y_c} \tag{4.20}$$

will satisfy the energy equation (4.18) identically. This is analogous to $u = \frac{\partial \psi}{\partial y_c}$, $v = -\frac{\partial \psi}{\partial x_c}$ which satisfies the continuity equation

$$\frac{\partial u}{\partial x_c} + \frac{\partial v}{\partial y_c} = 0.$$

It can be observed that the heat function is composed of two parts. The first term is the heat transmission via convection while the second term is via diffusion. Therefore, the path of the heat lines should give more indication of the energy transport than isotherms since the latter only indicates the second term, that is the diffusion. Note that the diffusion term will satisfy heat conduction equation and one would expect no further information than the constant

heat flux lines, perpendicular to the isotherms, where they were originally proposed.

The heat function H, is solved iteratively using

$$\frac{\partial^2 H}{\partial x_c^2} + \frac{\partial^2 H}{\partial y_c^2} = \rho C_p \left[\frac{\partial(uT)}{\partial y_c} - \frac{\partial(vT)}{\partial x_c}\right] \qquad (4.21)$$

which is obtained by differentiating eqns. (4.20) with respect to y_c and x_c and subtracting the resulting equations side by side. The right hand quantity in eqn. (4.21) is already known, therefore one has only to solve the Poisson equation. One difficulty in the method is the correction of the boundary conditions as the computation progresses using eqns. (4.20).

Eqns. (4.20) and (4.21) were also transformed to the previously defined mathematical plane and the resulting equation for eqn. (4.21) is similar to eqn. (C.3) with ψ replaced by H and W replaced by the source term on the right hand side of eqn. (4.21).

Eqns. (4.20) are after non-dimensionalization, become (noting that U = V = 0 at the walls),

$$\zeta\eta \frac{\partial H^+}{\partial \zeta} + \frac{\partial H^+}{\partial \eta} = \frac{-1}{\sqrt{1-\eta^2}} \frac{\partial \theta}{\partial \zeta} \qquad (4.22.a)$$

$$\frac{1}{\sqrt{1-\eta^2}} \frac{\partial H^+}{\partial \zeta} = \frac{\zeta\eta}{1-\eta^2} \frac{\partial \theta}{\partial \zeta} \qquad (4.22.b)$$

where we used the previously obtained result $\frac{\partial \theta}{\partial \eta} = 0$ in section 3 of this chapter. In the above equations, $H^+ = \frac{H}{qR}$.

At the interface the boundary condition for H^+ is computed from

$$\frac{\partial H^+}{\partial \eta} = Pr\sqrt{Gr^*_R}\, U\theta - \frac{1}{\sqrt{1-\eta^2}} \frac{\partial \theta}{\partial \zeta} \qquad (4.23)$$

The discretization of the above eqns. uses again central differences and will not be given here.

Applications of this method to the previously computed partially filled case show the conduction-convection dominated regimes of the flow field in Fig. 22. In Fig. 22.a near the walls, the heat lines are inclined in the flow direction hence the flow is convection dominated (see the flow field in Fig. 18.a). Near the interface however, these lines are perpendicular (especially at the corners) to the isotherms indicating that the heat transfer is by conduction only (Fig. 19.a). This is to be expected, since the inward velocities are very low near the corners where the flow moving up comes to a stop and turns towards the center. For later times, as the two rotating cells join, the heat flow in the cylinder becomes very complex. The steep gradients mentioned above still remain (Fig. 22.b) but in addition, two closed loops of heat lines form, resembling the flow lines of mass. Thus, we can say that these are showing the convection dominated regions.

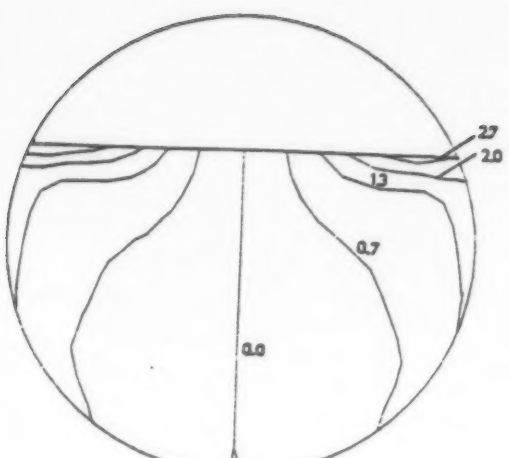

(a) t=0.7 mins

(b) t=4.6 mins

FIGURE 22. Heat lines for Pr=6380., Gr=114.

In summary, this method gives further insight to the heat transfer mechanism in addition to the well known isotherm visualization.

4.8 Conclusions

In this chapter, a numerical approach has been described utilizing a special coordinate transformation. The technique is capable of handling other geometries which meet the continuity requirements of the enclosing curve describing the container boundaries, except at the interface. This method is especially useful when there is an irregularity introduced by the partial filling of the container and of course, it is not limited to natural convection problems.

Experimental data available in the literature were compared to the computed results and reasonable agreement was obtained.

The simulation run for a partially filled cylinder revealed the interesting characteristics of the flow as well as the heat transfer mechanism. The simulation agreed qualitatively with the flow pattern in an experimental vessel displaying similar characteristics.

Finally, a recently introduced method was applied to the above case where it was possible to visualize the actual heat flow lines.

CHAPTER V

RECOMMENDATIONS AND CONCLUSIONS

Considering the initial objectives of the study, the present research is far from complete. The methodology applied is strictly valid for free convection flows and extension to two phase flow would require the solution of different model equations. However, the main lines of thought outlined here are invariant, that is if one solves two-phase boundary layer equations, one has to make a mass energy balance in the stratified layer, following developments similar to those outlined here. If one decides on the other hand, to integrate two phase flows in a partially filled geometry, the method outlined in Chapter IV is still valid with the necessary change in the model equations.

Thus for the most realistic approach to the present problem of a tank car simulation under intense radiation from a fire, one should solve three dimensional equations of two-phase turbulent flow where the liquid is continuously pressurized. The depressurization introduces other complex mechanisms such as flashing of the stratified liquid and should be handled in a different manner. The method suggested here may be applicable during those times where the valve is open but the vessel is being pressurized.

The technique introduced in Chapter IV can easily be applied to determine the effects of combined forced and natural convective flow in a horizontal, partially filled pipe, a case which has not been investigated so far apart from the special case of a completely filled pipe [36]. This has important practical applications in any situation where a liquid is transported horizontally in pipes subject to cooling or heating.

Another recommendation is an analytical study on the validity of boundary layer equations for a curved surface. As it seems, eqns. (1.8) to (1.10) remain in the same form for flow on either a concave or a convex surface. For example [19] and [29] have used them for flow around a horizontal cylinder whereas in [9] and this study they have been used for flow inside a concave surface. It can be shown that when $y = -y$ and $v = -v$, eqns. (1.8) to (1.10) remain the same, with the body force term still with a $\sin \phi$ term, in the direction of flow. Hence mathematically speaking these equations are applicable to both flows. However considering a horizontal cylinder, for a convex surface at $\phi = 0$ there will be no separation (assuming the wall is heated) whereas for a concave surface, separation is definitely present and the boundary layer forms at an angle $\phi > 0$. It may be that one of the most important conclusions of this work is to point out this difference and attempt to account for it as it was done in the

simplified stability theory. The author feels that this point deserves more attention than the actual solution of the equations. It is highly probable that this difference may be accounted for in the integral analysis with another method than that outlined in this study. For instance, one can run simulation computations for various Pr and Gr numbers, say by using the available program in Chapter IV and obtain a better representation for the velocity profiles as well as temperature, these may then be used to better represent the wall shear stress. This approach however is valid for laminar flow. For turbulent situations, the program itself must be modified and validated before attempting such a correction. Upon correcting the wall shear stresses obtained this way, it is now possible to obtain much better stability limits for boundary layer formation with correct profiles.

It is also recommended that the method introduced for the exact solution of integral equations be extended to cover cases with ambient fluid stratification. This problem so far has only been solved by numerical integration [15], [17], [28].

REFERENCES

[1] Venart, J.E.S., Sousa, A.C.M., Steward, F.R. and Lenard, J.G., "Tank Car Thermal Modelling", a Proposal to Supply and Services Canada: DSS File No. 09 SDT 8200-1-1540, Oct. 23, 1982, 52 pages.

[2] Ostrach, S., "Natural Convection in Enclosures", Advances in Heat Transfer, p. 161 (1972).

[3] Jaluria, Y., "Natural Convection Heat and Mass Transfer", Pergamon Press, (1980).

[4] Hellums, J.D. and Churchill, S.W., "Transient and Steady State, Free and Natural Convection, Numerical Solutions: Part I", AIChE J., 8, 690 (1962).

[5] Martini, W.R. and Churchill, S.W., "Natural Convection Inside A Horizontal Cylinder", AJChE J., 6, No. 2, p. 251, (1960).

[6] Brooks, I. and Ostrach, S., "An Experimental Investigation of Natural Convection in a Horizontal Cylinder", JFM, vol. 44, part 3, p. 545. (1970).

[7] Lai, M.W., Rubin, D. and Krempl, E., "Int. to Continuum Mechanics", Pergamon Press, (1979).

[8] Currie, I.G., "Fundamental Mechanics of Fluids", McGraw Hill, (1974).

[9] Maahs, G.H., "Transient Natural Convection Heat Transfer in a Horizontal Cylinder", Ph.D. Thesis, Univ. of Washington, (1964).

[10] Schlichting, H., "Boundary Layer Theory", 7th Ed., McGraw Hill, (1979).

[11] Venart, J.E.S., Sousa, A.C.M., Steward, F.R. and Prasad, R.C., "Experiments on the Physical Modelling of LPG Tank Car Under Accident Conditions", Symposium "Transport and Storage of LPG and LNG", Brugge, 7-9 May, 1984.

[12] Siegel, R., "Transient Free Convection From a Vertical Flat Plate", Transactions of the ASME, p. 347 (1956).

[13] Eckert, E.R.G., and Jackson, T.W., "Analysis of Turbulent Free Convection Boundary Layer on Flat Plate", NACA Report 1015, (1951).

[14] Zijnen, Van Der Hegge, "Measurements of the Velocity Distribution on the Boundary Layer Along a Plane Surface", abstracted in McAdams, Heat Transmission, p. 104, McGraw-Hill, (1942).

[15] Vliet, G.C., Brogan, J.J., Sheppard, T.S., Morse, F.H. and Hines, F.L., "Stratified Layer Flow Model: A Numerical Approach to Liquid Temperature Stratification", J. Spacecraft, Vol. 1, No. 6, p. 666, (1964).

[16] Suzuki, O. and Mizukami, A., "Unsteady Turbulent Natural Convection in a Tank", 1983 ASME WAM, Paper No. 83-WA/HT-2.

[17] Evans, L.B., Reid, R.C. and Drake, E.M., "Transient Natural Convection in a Vertical Cylinder", AIChE J., Vol. 14, No. 2, p. 251, (1968).

[18] Tuma, J.J., "Engineering Mathematics Handbook", McGraw Hill, (1970).

[19] Koh, J.C.Y., "Laminar Free Convection From a Horizontal Cylinder With Prescribed Surface Heat Flux", Int. J. Heat Mass Transfer, V. 7, p. 811, shorter communications, (1964).

[20] Ruder, J.M. and Little, A.D., "Stratification in a Pressurised Container with Side Wall Heating", AIAA, Vol. 2, No. 1, p. 135, (1964).

[21] Tellep, D.M. and Harper, E.Y., "Approximate Analysis of Propellant Stratification", AIAA J., V. 1, No. 8, p. 1954, (1963).

[22] Bailey, T., VandeKoppel, R. and Skartvedt, G., "Cryogenic Propellant Stratification Analysis and Test Data Correlation", AIAA J., V. 1, No. 7, p. 1657, (1963).

[23] Schinkel, W.M.M., Linthorst, S.J.M. and Hoogendoorn, C.J., "The Stratification in Natural Convection in Vertical Enclosures", JHT, V. 105, p. 267, (1983).

[24] Kimura, S. and Bejan, A., "The Boundary Layer Natural Convection Regime in a Rectangular Cavity With Uniform Heat Flux from the Side", JHT, V. 106, p. 99, (1984).

[25] Schwind, R.G. and Vliet, G.C., "Observations and Interpretations of Natural Convection and Stratification in Vessels", Heat Trans. and Fluid Mech. Inst., Proceedings of the 1963-64 Institute, p. 51, (1964).

[26] Tatom, J.W., Brown, W.H., Knight, L.H. and Coxe, E.F., "Analysis of Thermal Stratification of Liquid Hydrogen in Rocket Propellant Tanks", Adv. in Cryogenic Engineering, V. 9, p. 265, (1963).

[27] Jaguaribe, E.F. and Beasley, D.E., "Modelling of the Effective Thermal Conductivity and Diffusivity of a Packed Bed With Stagnant Fluid", Int. J. Heat and Mass Transfer, V. 27, No. 3, p. 399, (1984).

[28] Eichorn, R., "Natural Convection in a Thermally Stratified Fluid", Prog. Heat Mass Trans., Vol. 2, p. 241, (1969).

[29] Koh, J.C.Y. and Price, J.F., "Laminar Free Convection From a Non-Isothermal Cylinder", J.H.T., p. 237, (1965).

[30] Tatom, J.W., "Transient Turbulent Free Convection in a Container with Heating at the Sides Only", Proc. Heat Trans. and Fluid Mech. Inst., Northridge, Calif., p. 321,(1972).

[31] Adams, J.A. and Rogers, D.F., "Computer Aided Heat Transfer Analysis", McGraw Hill, p. 401, (1973).

[32] Roache, P.J., "Computational Fluid Dynamics", Hermosa Publishers, (1982).

[33] Aziz, K. and Hellums, J.D., "Numerical Solutions of the Three-Dimensional Equations of Motion for Laminar Natural Convection", Physics of Fluids, Vol. 10, No. 2, p. 314, (1967).

[34] Yao, L.S., "Natural Convection Along A Vertical Wavy Surface", JHT, Vol. 105, p. 465, (1983).

[35] Kimura, S. and Bejan, A., "The Heatline Visualization of Convective Heat Transfer", JHT, Vol. 105, p. 916, (1983).

[36] Patankar, S.V., Ramadhyani, S. and Sparrow, E.M., "Effect of Circumferentially Non-uniform Heating in Laminar Combined Convection in a Horizontal Tube", JHT, Vol. 100, p. 63, (1978).

APPENDIX A

In the calculations below, EXPLOSAFE (Style 2) will be assumed to be in a surrounding medium which is at rest. A typical cell is shown in Figure A.1.a with the nominal dimensions. The heat is conducted at the locations shown in Figure A.1.b which are the only contact points between two cells on two layers of EXPLOSAFE mesh.

The total amount of heat conducted through the metal-liquid cell can be written as:

$$Q_T = A_1 k_1 \frac{\Delta T}{t''} + A_2 k_2 \frac{\Delta T}{t''} \qquad (A.1)$$

where A_1 = effective fluid area = $(L_1 - 2\delta'')^2$;

A_2 = effective metal area = $4t''^2$;

k_1 = fluid thermal conductivity = 0.0886 W/mK;

k_2 = metal thermal conductivity = 204 Wm/K;

t'' = thickness of the metal = width of the metal; and

ΔT = average temperature difference across the metal-liquid cell.

The effective conductivity is:

$$k_{eff} = \frac{A_1}{A_T} k_1 + \frac{A_2}{A_T} k_2 \qquad (A.2)$$

where $A_T = L_2^2 + 4t''^2$

which results in $k_{eff} = 0.164$ W/mK.

This gives $\alpha_{eff} = 1.8\alpha_{Freon\ 11}$.

It is further assumed that the increase in the thickness of the thermal boundary layer is accompanied by the increase in the thickness of momentum boundary layer in the same proportion. That is,

$$\nu_{eff} = \nu_{Freon\ 11} \times 1.8$$

Since the flow is induced by the buoyancy forces, this assumption is justified as the liquid in the thermal layer will experience an upward buoyant force, thus increasing the thickness of the momentum boundary layer.

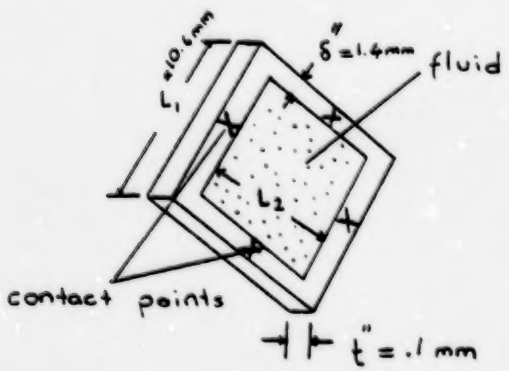

FIGURE A.1.a A representative cell of the EXPLOSAFE mesh.

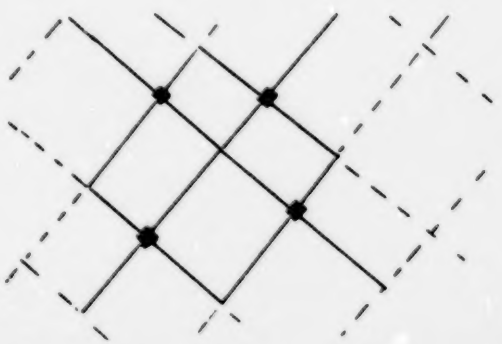

FIGURE A.1.b Four points of metal to metal contact between two sheets of EXPLOSAFE in a typical cell.

APPENDIX B

Eqns. (1.8) to (1.10) are non-dimensionalized and written in the following form:

$$f_{\bar{\eta}} f_{\bar{\eta}\phi} - f_{\phi} f_{\bar{\eta}\bar{\eta}} = \theta \sin \phi + f_{\bar{\eta}\bar{\eta}\bar{\eta}} \tag{B.1}$$

$$f_{\bar{\eta}} \theta_{\phi} - f_{\phi} \theta_{\bar{\eta}} = \frac{1}{Pr} \theta_{\bar{\eta}\bar{\eta}} - f_{\bar{\eta}} A' \tag{B.2}$$

using

$$u = \frac{\partial \psi}{\partial y}, \quad v = -\frac{\partial \psi}{\partial x}, \quad \phi = \frac{x}{R}, \quad \bar{\eta} = \frac{y}{R} Gr_R^{*1/5}$$

$$\theta = k \frac{(T-T_{\infty})}{qR} Gr_R^{*1/5}, \quad \psi = \nu Gr_R^{*1/5} f(\phi, \bar{\eta}) \tag{B.3}$$

$$A = \frac{k}{qR} Gr_R^{*1/5} T_{\infty}(x)$$

The power series expansion suggested by [29] is used with a constant heat flux boundary condition:

$$\begin{aligned} f(\phi, \bar{\eta}) &= \phi f_0 + \phi^3 f_1 + \phi^5 f_2 + \ldots \\ \theta(\phi, \bar{\eta}) &= \theta_0 + \phi^2 \theta_1 + \phi^4 \theta_2 + \ldots \end{aligned} \tag{B.4}$$

Substituting eqn. (B.4) in (B.1) and (B.2), noting that f_0, f_1, ..., θ_0, θ_1, ... are functions of $\bar{\eta}$ only, and expanding the sin ϕ term in power series, we obtain an

infinite set of differential equations for like powers of ϕ as follows:

$$f_0''' = (f_0')^2 - f_0 f_0'' - \theta_0$$

$$\theta_0'' = -\Pr\, f_0\, \theta_0' \tag{B.5}$$

$$f_1''' = 4f_0' f_1' - f_0' f_1'' - 3f_1 f_0'' - \theta_0/6 - \theta_1$$

$$\theta_1'' = \Pr[2f_0'\theta_1 - f_0\theta_1' - 3f_1\theta_0' + f_0'] \tag{B.6}$$

$$f_2''' = 6f_0' f_2' + 3(f_1')^2 - f_0 f_2'' - 3f_1 f_1'' - 5f_0'' f_2 - \frac{\theta_0}{120}$$

$$+ \frac{\theta_1}{6} - \theta_2 \tag{B.7}$$

$$\theta_2'' = \Pr[4f_0'\theta_2 + 2f_1'\theta_1 - f_0\theta_2' - 3f_1\theta_1' - 5f_2\theta_0' + f_1']$$

subject to:

at $\bar{\eta} = 0$; $f_0 = f_0' = f_1 = f_1' = f_2 = f_2' = 0$;

$$\theta_0' = -1,\ \theta_1' = \theta_2' = 0$$

at $\bar{\eta} \to \infty$; $f_0' \to 0,\ f_1' \to 0,\ f_2' \to 0$;

$$\theta_0 \to 0,\ \theta_1 \to 0,\ \theta_2 \to 0.$$

One can write as many of these equations as necessary until sufficient accuracy is achieved. It has been assumed

in eqns. (B.5) to (B.7) that

$$A = \phi + \phi^2/2.$$

These eqns. were solved using a second order Runge-Kutta method where Nachsteim-Swigert scheme is used to satisfy the asymptotic boundary conditions as outlined in [31].

Other values of A that were considered are:

$$A = \phi + \phi^2$$

$$A = \phi + \phi^2/4$$

The solutions will not be tabulated here but two examples fo_ A = 0 and $A = \phi + \phi^2/2$ will be given in Figs. B.1 and B.2 where the first three solutions for velocity profiles are represented in non-dimensional form.

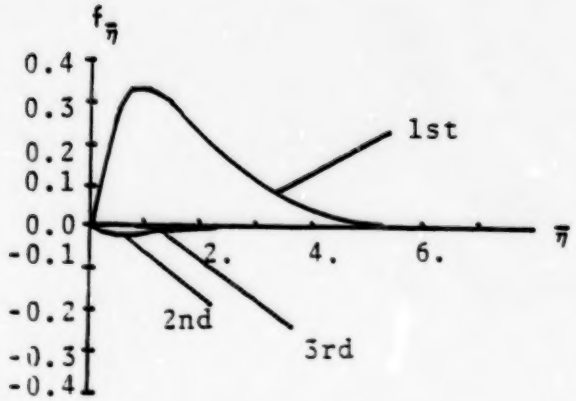

FIGURE B.1 First three solutions for the dimensionless velocity profiles, no external stratification.

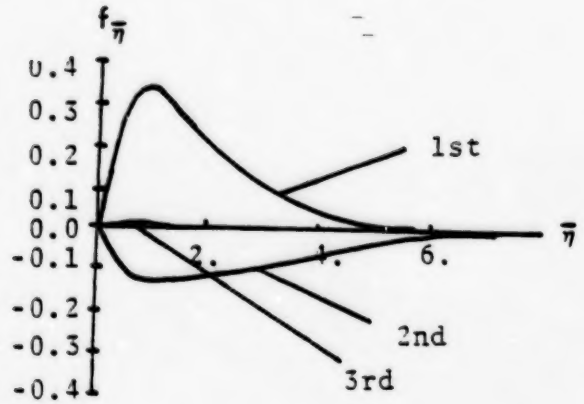

FIGURE B.2 First three solutions for the dimensionless velocity profiles for $A=\phi+\phi^2/2$.

APPENDIX C

Equations (4.1) can be rewritten using eqns. (4.5) and (4.6) as follows:

Vorticity Transport Equation:

$$\frac{U}{(1-\eta^2)^{\frac{1}{2}}}\frac{\partial W}{\partial \zeta} + V\left(\frac{\zeta\eta}{1-\eta^2}\frac{\partial W}{\partial \zeta} + \frac{\partial W}{\partial \eta}\right) = \frac{1}{(1-\eta^2)^{\frac{1}{2}}}\frac{\partial \theta}{\partial \zeta}$$

$$+ \frac{1}{\sqrt{Gr_R}}\left\{\frac{\zeta(1+2\zeta^2)}{(1-\eta^2)^2}\frac{\partial W}{\partial \zeta} + \left(\frac{1}{1-\eta^2} + \frac{\zeta^2\eta^2}{(1-\eta^2)^2}\right)\frac{\partial^2 W}{\partial \zeta^2}\right.$$

$$\left. + \frac{\partial^2 W}{\partial \eta^2} + \frac{2\zeta\eta}{1-\eta^2}\frac{\partial^2 W}{\partial \zeta \partial \eta}\right\} \qquad (C.1)$$

Energy Equation:

$$\frac{U}{(1-\eta^2)^{\frac{1}{2}}}\frac{\partial \theta}{\partial \zeta} + V\left(\frac{\zeta\eta}{1-\eta^2}\frac{\partial \theta}{\partial \zeta} + \frac{\partial \theta}{\partial \zeta}\right) = \frac{1}{Pr\sqrt{Gr_R}}\left\{\frac{\zeta(1+2\eta^2)}{(1-\eta^2)^2}\frac{\partial \theta}{\partial \zeta}\right.$$

$$\left. + \left(\frac{1}{1-\eta^2} + \frac{\zeta^2\eta^2}{(1-\eta^2)^2}\right)\frac{\partial^2 \theta}{\partial \zeta^2} + \frac{\partial^2 \theta}{\partial \eta^2} + \frac{2\zeta\eta}{1-\eta^2}\frac{\partial^2 \theta}{\partial \zeta \partial \eta}\right\} \qquad (C.2)$$

Stream Function-Vorticity Equation:

$$\zeta\frac{(1+2\eta^2)}{(1-\eta^2)^2}\frac{\partial \psi}{\partial \zeta} + \left(\frac{1}{1-\eta^2} + \frac{\zeta^2\eta^2}{(1-\eta^2)^2}\right)\frac{\partial^2 \psi}{\partial \zeta^2} + \frac{\partial^2 \psi}{\partial \eta^2} + \frac{2\zeta\eta}{1-\eta^2}\frac{\partial^2 \psi}{\partial \zeta \partial \eta} = -W \qquad (C.3)$$

Velocity Relations:

$$U = \frac{\zeta\eta}{1-\eta^2}\frac{\partial\psi}{\partial\zeta} + \frac{\partial\psi}{\partial\eta}, \quad V = -\frac{1}{(1-\eta^2)^{\frac{1}{2}}}\frac{\partial\psi}{\partial\zeta} \qquad (C.4)$$

APPENDIX D

The discretized equations are: (for $\Delta\zeta = \Delta\eta$)

Vorticity Transport Equation:

$$C_1 W_{i,j} = C_2 W_{i+1,j} + C_3 W_{i-1,j} + C_4 W_{i,j+1} + C_5 W_{i,j-1} + C_6 + C_7 \qquad (D.1)$$

where

$$C_1 = \frac{2}{\sqrt{Gr_R}} \left(\frac{1}{1-\eta^2} \frac{\zeta^2\eta^2}{(1-\eta^2)^2}\right) + \frac{2}{\sqrt{Gr_R}}$$

$$C_2 = -\frac{U_{i,j}\,\Delta\zeta}{2(1-\eta^2)^{\frac{1}{2}}} - \frac{V_{i,j}\,\zeta\eta\Delta\zeta}{2(1-\zeta^2)} + \frac{(1+2\eta^2)\,\Delta\zeta}{2\sqrt{Gr_R}\,(1-\eta^2)^2}$$

$$+ \frac{1}{\sqrt{Gr_R}} \left(\frac{1}{1-\eta^2} + \frac{\zeta^2\eta^2}{(1-\eta^2)^2}\right)$$

$$C_3 = \frac{U_{i,j}\,\Delta\zeta}{2(1-\eta^2)^{\frac{1}{2}}} + \frac{V_{i,j}\,\zeta\eta\Delta\zeta}{2(1-\eta^2)} - \frac{\Delta\zeta}{2\sqrt{Gr_R}} \left[\zeta \frac{(1+2\eta^2)}{(1-\eta^2)^2}\right]$$

$$+ \left(\frac{1}{1-\eta^2} \frac{\zeta^2\eta^2}{(1-\eta^2)^2}\right) \frac{1}{\sqrt{Gr_R}}$$

$$C_4 = -\frac{V_{i,j}\,\Delta\zeta}{2} + \frac{1}{\sqrt{Gr_R}}, \quad C_5 = \frac{V_{i,j}\,\Delta\zeta}{2} + \frac{1}{\sqrt{Gr_R}}$$

$$C_6 = \frac{\Delta\zeta}{2(1-\eta^2)^{\frac{1}{2}}} \left[\theta_{i+1,j} - \theta_{i-1,j}\right]$$

$$C_7 = \frac{2\zeta\eta}{4\sqrt{Gr_R}\,(1-\eta^2)}\,(W_{i+1,j+1} - W_{i-1,j+1} - W_{i+1,j-1} + W_{i-1,j-1})$$

Energy Equation:

This is similar to (D.1) with $\sqrt{Gr_R}$ replaced by $Pr\sqrt{Gr_R}$ and $C_6 \equiv 0$ (no source term). (D.2)

Stream Function-Vorticity Equation:

$$\psi_{i,j} = \psi_{i,j} + \frac{\omega_0}{C_1}\,(\Delta\zeta^2 W_{i,j} - C_1\psi_{i,j} + C_2\psi_{i+1,j} + C_3\psi_{i-1,j} + \psi_{i,j-1} + \psi_{i,j+1} + C_4) \qquad (D.3)$$

where

$$C_1 = 2 + 2\left(\frac{1}{1-\eta^2} + \frac{\zeta^2\eta^2}{(1-\eta^2)^2}\right)$$

$$C_2 = \frac{(1+2\eta^2)\Delta\zeta}{2(1-\eta^2)^2} + \left(\frac{1}{1-\eta^2} + \frac{\zeta^2\eta^2}{(1-\eta^2)^2}\right)$$

$$C_3 = \frac{-\zeta(1+2\eta^2)\Delta\zeta}{2(1-\eta^2)^2} + \frac{1}{1-\eta^2} + \frac{\zeta^2\eta^2}{(1-\eta^2)^2}$$

$$C_4 = \frac{\zeta\eta}{2(1-\eta^2)}\,(\psi_{i+1,j+1} - \psi_{i-1,j+1} - \psi_{i+1,j-1} + \psi_{i-1,j-1})$$

APPENDIX E

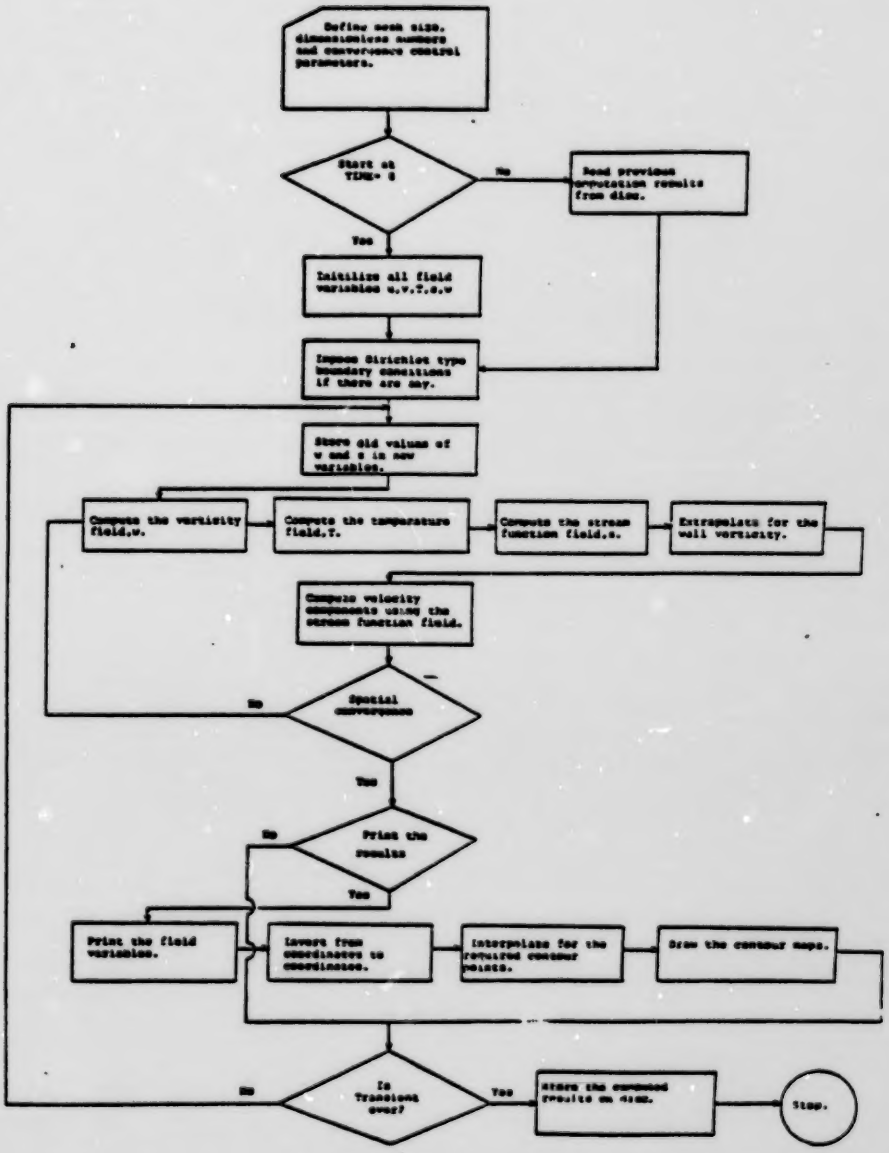
Define mesh size, dimensionless numbers and convergence control parameters.
Start at TIME= 0
No
Read previous computation results from disc.
Yes
Initilize all field variables u,v,T,s,w
Impose Dirichlet type boundary conditions if there are any.
Store old values of w and s in new variables.
Compute the vorticity field,w.
Compute the temperature field,T.
Compute the stream function field,s.
Extrapolate for the wall vorticity.
Compute velocity components using the stream function field.
Spatial convergence
No
Yes
Print the results
No
Yes
Print the field variables.
Lowers from coordinates to coordinates.
Interpolate for the refined contour points.
Draw the contour maps.
Is Transient over?
No
Yes
Store the computed results on disc.
Stop.